

Transient Response and Adjustment Timescales of Channel Width and Angle of Valley-Side Slopes to Accelerated Incision

Naoya Takahashi¹, J. Bruce H. Shyu², Shinji Toda¹, Yuki Matsushi³, Ryoga Ohta⁴, and Hiroyuki Matsuzaki⁵

¹Tohoku University

²National Taiwan University

³DPRI, Kyoto University

⁴Chuo University

⁵University of Tokyo

January 20, 2023

Abstract

Studying bedrock rivers during their transient states helps understand the response of a fluvial system to changed boundary conditions. Although studies show how river form adjusts to changes in incision or rock uplift rates, field constraints on the timescale of this adjustment are limited. We present a method that uses knickpoint travel time to estimate the adjustment times of channel width and angle of valley-side slopes to accelerated incision. The travel time of knickpoints between their current positions and the points where changes in width or hillslope angle have just finished represents the time required for morphological adjustment after knickpoint passage. We documented channel slopes, channel widths, and hillslope angles along six rivers that cross an active normal fault in Iwaki, Japan, and identified river sections in a transient state. Channel slopes and basin-averaged erosion rates determined from ¹⁰Be concentrations are distinct between rivers near and distant from the fault, suggesting that past increases in fault throw rates triggered the knickpoint formation and the observed transient response. Adjustment time depends on the slope exponent in the detachment-limited model and is 2–5 times greater for channel width than hillslope angle, indicating that catchment adjustment times can be much longer than times predicted only by knickpoint travel time. The fact that channel slope, channel width, and hillslope angle have distinct adjustment times underlines the importance of correctly identifying river sections that are fully adjusted to the new boundary conditions when inferring erosion or relative uplift rates for bedrock rivers.

1 **Transient Response and Adjustment Timescales of Channel Width and Angle of** 2 **Valley-Side Slopes to Accelerated Incision**

3
4 **Naoya Takahashi^{1,*}, J. Bruce H. Shyu^{2,*}, Shinji Toda³, Yuki Matsushi⁴, Ryoga Ohta⁵, and**
5 **Hiroyuki Matsuzaki⁶**

6 ¹ Department of Earth Science, Tohoku University, 6-3, Aramaki Aza-Aoba, Aoba-ku, Sendai 980-8578, Japan

7 ² Department of Geosciences, National Taiwan University, No. 1, Sec. 4, Roosevelt Road, Taipei 106, Taiwan,
8 ROC

9 ³ International Research Institute of Disaster Science (IRIDeS), Tohoku University, Aoba, 468-1, Aoba, Sendai
10 980-0845, Japan

11 ⁴ Disaster Prevention Research Institute, Kyoto University, Gokasho, Uji city, Kyoto 611-0011, Japan

12 ⁵ Faculty of Science and Engineering, Chuo University, 1-13-27, Kasuga, Bunkyo-ku, Tokyo 112-8551, Japan

13 ⁶ Micro Analysis Laboratory, Tandem Accelerator (MALT), The University Museum, The University of Tokyo,
14 2-11-16, Yayoi, Bunkyo-ku, Tokyo 113-0032, Japan

15 Corresponding author:

16 Naoya Takahashi (naoya.takahashi.c5@tohoku.ac.jp) (orcid.org/0000-0003-4196-1409)

17 J. Bruce H. Shyu (jbhs@ntu.edu.tw) (orcid.org/0000-0002-2564-3702)

19 **Key Points:**

- 20
- 21 • We use knickpoint travel time to estimate the time between knickpoint passage and
22 channel/hillslope adjustments to accelerated incision.
 - 23 • The adjustment of channel width after the passage of a knickpoint takes 2–5 times longer
24 than the adjustment of valley-side slope.
 - 25 • Adjustment of the entire river basin takes much longer than the time a knickpoint takes to
26 travel upstream to the channel heads.

27 Abstract

28 Studying bedrock rivers during their transient states helps understand the response of a fluvial
29 system to changed boundary conditions. Although studies show how river form adjusts to
30 changes in incision or rock uplift rates, field constraints on the timescale of this adjustment are
31 limited. We present a method that uses knickpoint travel time to estimate the adjustment times of
32 channel width and angle of valley-side slopes to accelerated incision. The travel time of
33 knickpoints between their current positions and the points where changes in width or hillslope
34 angle have just finished represents the time required for morphological adjustment after
35 knickpoint passage. We documented channel slopes, channel widths, and hillslope angles along
36 six rivers that cross an active normal fault in Iwaki, Japan, and identified river sections in a
37 transient state. Channel slopes and basin-averaged erosion rates determined from ^{10}Be
38 concentrations are distinct between rivers near and distant from the fault, suggesting that past
39 increases in fault throw rates triggered the knickpoint formation and the observed transient
40 response. Adjustment time depends on the slope exponent in the detachment-limited model and
41 is 2–5 times greater for channel width than hillslope angle, indicating that catchment adjustment
42 times can be much longer than times predicted only by knickpoint travel time. The fact that
43 channel slope, channel width, and hillslope angle have distinct adjustment times underlines the
44 importance of correctly identifying river sections that are fully adjusted to the new boundary
45 conditions when inferring erosion or relative uplift rates for bedrock rivers.

46

47 Plain Language Summary

48 Bedrock rivers adjust their forms in response to changes in their boundary conditions, such as
49 underlying rock types, climate, and tectonics, which means that establishing their quantitative
50 relationships between these boundary conditions may enable us to infer rates of erosion or
51 relative uplift from river morphologies. Although it is well known how river and hillslope forms
52 adjust after an increase in erosion rates, the timescale of these adjustments is difficult to
53 constrain in an actual landscape. This study presents a method to estimate the adjustment times
54 of channel width and hillside slope angles along the sides of a valley. We studied a set of rivers
55 that cross an active normal fault and documented the variations of channel and hillslope forms
56 along their courses. These rivers are now changing their shapes after motion on the fault has

57 increased their erosion rates. Our analysis shows that channel width likely takes 2–5 times longer
58 to complete its adjustment than does the hillslope angle. Our findings show that channel slope,
59 channel width, and hillslope angle all have distinct adjustment times. It may take longer than
60 previously thought for an entire river system to adjust to new boundary conditions.

61

62 **1. Introduction**

63 Because the incision of rivers into bedrock is a major element in the formation of
64 mountain landscapes, quantifying incision rates and their relationships with external forces is
65 important for understanding landscape evolution. The morphology of channels and hillslopes is
66 closely related to erosion rates, and a long history of research has gone into establishing their
67 functional relationships (e.g., Ahnert, 1970; Wobus et al., 2006a; Roering et al., 2007; Kirby &
68 Whipple, 2012). A sudden increase in the rate of base-level fall (i.e., relative uplift) can enhance
69 local incision rates and may generate a knickpoint that migrates upstream (e.g., Whipple &
70 Tucker, 1999; Crosby & Whipple, 2006). As it does so, channels and hillslopes along its passage
71 gradually adjust their forms to the accelerated incision rates. Knickpoints are common in
72 tectonically active areas, and thus knowledge of the transient response of rivers to an increase in
73 incision rates may enable researchers to infer a region's erosional or tectonic history from river
74 morphologies.

75 Channel slope, channel width, and the angle of valley-side slopes are closely related to
76 channel incision rates, and many studies have focused on quantifying relationships between
77 morphologies of channel and hillslope and rates of incision or relative uplift (e.g., Whipple &
78 Tucker, 1999; Snyder et al., 2000; Lavé & Avouac, 2001; Roering et al., 2001; Montgomery &
79 Brandon, 2002; Reinhardt et al., 2007; Yanites & Tucker, 2010). The channel steepness index,
80 expressing the channel slope normalized by upstream drainage area (e.g., Snyder et al., 2000),
81 increases after the passage of a knickpoint in response to an increase in incision rates. Channel
82 steepness downstream from the migrating knickpoint is assumed to reach a new steady-state
83 value and is often positively correlated with uplift rates (e.g., Kirby & Whipple, 2012; Regalla et
84 al., 2013; Chen et al., 2015; Gallen & Wegmann, 2017). Channel width can become wider or
85 narrower in response to increased incision rates or be insensitive to incision rates (e.g., Lavé &
86 Avouac, 2001; Snyder et al., 2003; Yanites & Tucker, 2010). According to a numerical study

87 that considered the effects of sediment cover, channel narrowing occurs after the knickpoint
88 passage, but as the knickpoint travels upstream the local sediment supply continues to increase,
89 resulting in gradual widening of the channel (Yanites, 2018). A similar width adjustment was
90 observed in a flume experiment (Baynes et al., 2022). Hillslope morphology is set by river
91 incision at its base. The hillslope angle increases with incision rates until it reaches a threshold
92 angle, above which it becomes insensitive to incision rate (e.g., Montgomery & Brandon, 2002).
93 The threshold angle, usually $\sim 30^\circ$ – 40° , is reached at relatively slow incision rates of 0.2–1.0
94 mm/yr (e.g., Montgomery & Brandon, 2002; Ouimet et al., 2009; DiBiase et al., 2012).

95 Whereas many studies have examined how river morphologies adjust to changes in
96 incision rates, relatively few have attempted to quantify the adjustment timescales of channels
97 and hillslopes to accelerated incision. Such studies require a chronology that specifies the times
98 at which these morphological adjustments begin and end. However, in actual landscapes, it is
99 very difficult to constrain those timings except for channel slope (e.g., Crosby & Whipple, 2006;
100 Whittaker & Boulton, 2012). The arrival of a knickpoint triggers a change in channel slope from
101 which a rate of knickpoint retreat can be calculated (e.g., Whipple & Tucker, 1999; Royden &
102 Perron, 2013). Therefore, when the time and place a knickpoint is generated are known, the
103 timescale of channel slope adjustment can be estimated based on the knickpoint's travel distance
104 and travel speed (e.g., DiBiase et al., 2015).

105 The adjustment timescales of channel width and hillslope, unlike that for channel slope,
106 are difficult to estimate by using field evidence. Instead, they have been studied by numerical
107 modeling (e.g., Roering et al., 2001; Mudd & Furbish, 2007; Yanites, 2018; Turowski, 2020).
108 Yanites (2018), modeling the evolution of channel width after knickpoint passage, showed that
109 the full adjustment could take 10^5 – 10^6 years. Roering et al. (2001) used sediment transport
110 models on hillslopes to estimate the adjustment time of valley-side slopes to a change in base-
111 level lowering rates. The model parameters used in these studies were based on field
112 observations. However, we still know little about the actual adjustment timescales of channel
113 width and hillslopes, due to the difficulties in constraining when those adjustments started and
114 finished.

115 This paper presents a method to quantify the adjustment timescales of channel width and
116 the angle of valley-side slopes. We applied the method to bedrock rivers that cross an active

117 normal fault near the city of Iwaki, Japan. Because changes in channel width and hillslope follow
118 the passage of a knickpoint, we can use knickpoint travel times to estimate three quantities at any
119 given location: response time, the time between the start and finish of a morphological
120 adjustment; delay time, the lag time between the knickpoint arrival and the start of
121 morphological adjustment; and adjustment timescale, the sum of response and delay times,
122 representing the time between knickpoint passage and the finish of adjustment. Therefore, for the
123 adjustment of channel slopes, the delay time at a given location is always zero, the response time
124 is the time from the knickpoint passage until the channel slope attains a steady-state value, and
125 the adjustment time equals the response time. We investigated channel slope, channel width, and
126 hillslope angle along trunk streams and identified points at which morphological adjustments
127 started and finished. Because we cannot know exactly when channel or hillslope adjustments
128 have finished, we defined the end of adjustment as the condition where channel and hillslope
129 forms are indistinguishable from those presumably at a steady state. We then calculated
130 knickpoint travel times and estimated the response and delay times of channel width and
131 hillslope angle. We use these results to discuss how the channel width and the angle of valley-
132 side slopes change following an increase in channel incision rates, highlighting the need to
133 inspect channels and hillslopes along a trunk stream and its tributaries when inferring incision or
134 tectonic histories from river morphologies.

135

136 **2. Background**

137 **2.1 Tectonic and Geologic Background**

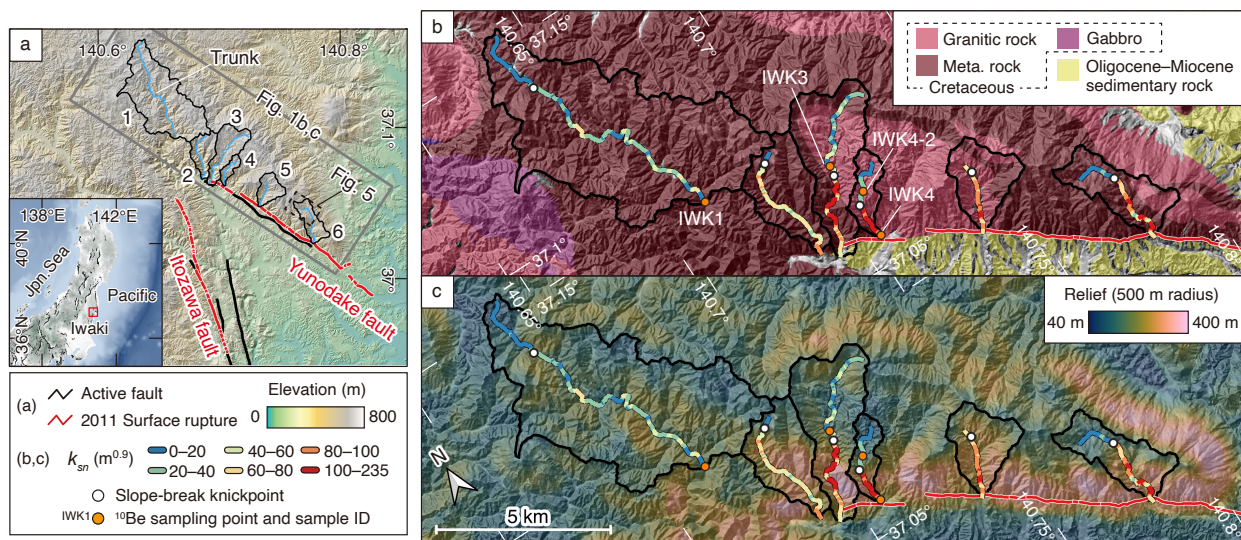
138 Iwaki is in the Tohoku region of northeastern Japan, which is subjected to E-W
139 compression due to westward subduction of the Pacific plate under the Eurasia plate (Figure 1a).
140 Although most earthquakes in Tohoku are characterized by reverse faulting, analysis of
141 microearthquakes during 2003–2010 has revealed that the Iwaki area has been in an extensional
142 stress regime since before the 11 March 2011 Mw 9.0 Tohoku-Oki earthquake (Imanishi et al.,
143 2012). Shortly after the Tohoku-Oki event, a normal-faulting event of Mw 6.6 occurred in Iwaki
144 on 11 April 2011. This earthquake produced surface ruptures along the Yunodake and Itozawa
145 faults (Figure 1a) (e.g., Fukushima et al., 2013; Toda & Tsutsumi, 2013). The Yunodake and
146 Itozawa faults are normal faults dipping SW and WSW, respectively, that form a half-graben

147 between them (Mitsui, 1971), suggesting that this area has experienced extension on a geological
 148 timescale. The vertical slip rate of the Yunodake fault is unknown. A paleoseismic trenching
 149 study (Miyashita, 2018) showed that three surface-rupturing earthquakes including the 2011
 150 event occurred on the Yunodake fault within the last 7 ky. If we assume that each of these
 151 produced vertical displacements similar to that in 2011 (~80 cm: Toda & Tsutsumi, 2013), a
 152 rough estimate of the fault throw rate is ~0.34 mm/yr.

153 Bedrock around the Yunodake fault consists of metamorphic and granitic rocks of
 154 Cretaceous age and sedimentary rocks of Miocene age (e.g., Kubo et al., 2007) (Figure 1b).
 155 Cretaceous metamorphic rocks include siliceous, mafic, pelitic and calcareous rocks (Kano et al.,
 156 1973; Hiroi et al., 1987; Kubo et al., 2007). Cretaceous granodiorite and porphyritic granodiorite
 157 occur along the middle and eastern part of the Yunodake fault (Kubo et al., 2007). Miocene
 158 sedimentary rocks southwest of the Yunodake fault include marine and nonmarine clastic rocks
 159 (Kubo et al., 2007) that overlie Cretaceous metamorphic rocks (Mitsui, 1971).

160 We focus on six trunk streams, numbered 1 through 6, along the Yunodake fault (Figure
 161 1). Their drainage areas range from 1.6 to 24.1 km² and average 7.4 km² (Table S1). The
 162 substrates are either metamorphic or granitic rocks. Riverbeds are typically covered with gravel
 163 in reaches of metamorphic rocks and with sand in reaches of granitic rocks. Although Basins 2–6
 164 intersect with or are very close to the fault, Basin 1 does not cross the fault. Basins 2–6 are
 165 characterized by steeper downstream reaches and gentler upstream reaches of smaller relief
 166 (Figure 1c).

167



168

169 **Figure 1.** (a) Location and topography of the study area. Drainage basins and their trunk streams
 170 are labeled with their identification number (1–6). The inset map shows topography and active
 171 fault traces in eastern Japan. Active fault traces are from Nakata and Imaizumi (2002). Surface
 172 rupture traces are after Toda and Tsutsumi (2013). (b) Geologic map around the Yunodake fault
 173 (Kubo et al., 2007; Geological Survey of Japan, 2020). (c) Topographic relief in the area of (b)
 174 within circular windows of 500 m radius.

175

176 **2.2. Channel and Hillslope Morphology**

177 **2.2.1. Channel Slope**

178 In a stream at steady state, local channel slope (S) is a function of flow discharge, which
 179 is commonly represented by upstream drainage area (A):

$$180 \quad S = k_s A^{-\theta}, \quad (1)$$

181 where k_s is a steepness index and θ is a concavity index (e.g., Flint, 1974; Snyder et al., 2000).

182 Equation (1) holds only above a critical drainage area ($A > A_{\text{crt}}$), at which the dominant
 183 erosional process changes from colluvial (debris flows) to fluvial processes (e.g., Montgomery &
 184 Fournelle-Georgiou, 1993; Stock & Dietrich, 2003). In drainage areas smaller than A_{crt} , channel
 185 slope either increases with or is independent of drainage area. The concavity index typically
 186 ranges between 0.4 and 0.6 (e.g., Kirby & Whipple, 2012).

187 The standard stream power model (e.g., Howard & Kerby, 1983) predicts a relation
 188 between channel slope and upstream drainage area similar to equation (1):

$$189 \quad S = (E/K)^{1/n} A^{-m/n}, \quad (2)$$

190 where E is a local erosion rate, K is erodibility, m is related to the dominant erosion process and
 191 n is related to the hydraulic scaling relationships among channel width, flow discharge, and
 192 drainage area (e.g., Whipple & Tucker, 1999). From equations (1) and (2), under a steady state
 193 where local erosion rates match local uplift rates (U), channel steepness can be written as

$$194 \quad k_s = (E/K)^{1/n} = (U/K)^{1/n}. \quad (3)$$

195 Because the concavity index is independent of uplift rates when the gradient of local uplift rates
 196 within a basin has a negligible impact on a channel profile (e.g., Snyder et al., 2000), a fixed
 197 concavity index ($\theta = \theta_{\text{ref}}$, equation (1)) is used to calculate k_s , and the resulting channel
 198 steepness is termed a normalized steepness index (k_{sn} ; Wobus et al., 2006a).

199 A sustained increase in the rate of base-level lowering can generate a knickpoint (or a
 200 knickzone). This knickpoint propagates upstream and separates the longitudinal river profile into
 201 two segments: an adjusted segment downstream with higher steepness and a pre-adjusted
 202 segment upstream with lower steepness. This mobile knickpoint, called a slope-break knickpoint
 203 (e.g., Whipple et al., 2013), is readily distinguished from a stationary knickpoint (vertical-step
 204 knickpoint) that has different origins, such as a local decrease in bed erodibility associated with
 205 resistant substrates.

206

207 **2.2.2. Channel Width**

208 The channel width (W) of bedrock rivers is a power function of drainage area (e.g.,
 209 Montgomery & Gran, 2001):

$$210 \quad W = k_w A^b, \quad (4)$$

211 where k_w (unit: m^{1-2b}) is a wideness index (e.g., Allen et al., 2013) and b is a positive exponent
 212 that is typically 0.3–0.5 at a steady state (e.g., Whipple, 2004). A larger wideness index indicates
 213 a wider channel. Similar to k_{sn} and θ_{ref} , k_w calculated using a fixed value of b (b_{ref}) is a
 214 normalized wideness index (k_{wn}). An adjustment in channel width in response to accelerated
 215 incision should appear as a break in the hydraulic scaling of equation (4) or a change in average
 216 k_{wn} values with distance along the stream.

217

218 **2.2.3. Angle of Valley-Side Slopes**

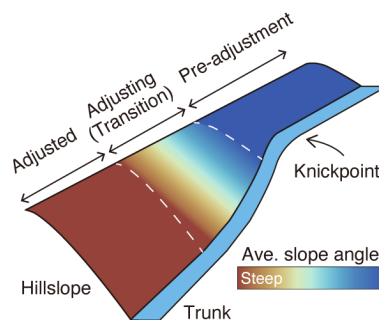
219 In mountainous landscapes, drainage basins consist primarily of hillslopes, and material
 220 transport on hillslopes dictates the sediment supply to channels (e.g., Roering, 2008). Following
 221 the passage of a knickpoint produced by increased base-level lowering rates, hillslopes become
 222 steeper such that hillslope lowering keeps pace with channel incision (e.g., Roering et al., 2001).
 223 A downstream increase in hillslope angle is expected downstream of a slope-break knickpoint,
 224 and our analysis focused on this transition.

225

226 **2.3. Knickpoint Travel Speed and the Timescales of Channel Width and Hillslope Angle** 227 **Adjustments**

228 Following the passage of a slope-break knickpoint, the channel width and the angle of
 229 valley-side slopes are expected to change until the local incision rate matches the local uplift
 230 rate. This morphological adjustment is characterized by a response time and a delay time, as
 231 defined in section 1. We estimated the response and delay times for channel width and hillslope
 232 angle based on knickpoint travel time.

233 Figure 2 schematically illustrates the response of a valley-side slope to accelerated
 234 incision. Hillslopes downstream from the knickpoint can be divided into three sections
 235 representing the phases of morphological adjustment. The pre-adjustment hillslope extends from
 236 upstream to slightly downstream of the knickpoint, and its angle reflects the incision rate before
 237 acceleration. The adjusted hillslope, well downstream from the knickpoint, has an angle that is
 238 fully adjusted to the accelerated incision. Between these two sections is the adjusting hillslope,
 239 with an angle that is currently changing in response to the accelerated incision. Because the
 240 knickpoint propagates upstream, its travel time from the boundary between the pre-adjustment
 241 and adjusting sections to the current knickpoint position represents the delay time. The
 242 knickpoint travel time from this boundary to the boundary between the adjusting and adjusted
 243 sections is the response time. The adjustment time is the sum of the response and delay times.
 244



245
 246 **Figure 2.** Schematic diagram of the right bank of a stream showing the response of hillslope
 247 angle to accelerated incision. The hillslope angle starts to change at the boundary between the
 248 pre-adjustment and adjusting sections and finishes at the boundary between the adjusting and
 249 adjusted sections.

250

251 Following a sustained increase in incision rates, knickpoint travel distance in χ -space is
 252 written as (Royden & Perron, 2013; Mitchell & Yanites, 2019):

$$\chi_{kp}(t) = \begin{cases} \frac{nU_{ini}}{\left(\frac{U_{ini}}{K}\right)^{\frac{1}{n}} A_0^{-\frac{m}{n}}} t & n < 1 \quad (5a) \\ KA_0^{\frac{m}{n}} t & n = 1 \quad (5b) \\ \frac{U_{fin} - U_{ini}}{\left(\left(\frac{U_{fin}}{K}\right)^{\frac{1}{n}} - \left(\frac{U_{ini}}{K}\right)^{\frac{1}{n}}\right) A_0^{-\frac{m}{n}}} t & n > 1 \quad (5c) \end{cases}$$

254 where $\chi_{kp}(t)$ is a χ of a mobile knickpoint at time t since knickpoint generation. A_0 is a
 255 reference drainage area, which was set at 1 in this study. Subscripts *ini* and *fin* represent the
 256 initial and final steady state, respectively; thus U_{ini} and U_{fin} are initial and final uplift rates
 257 ($U_{ini} < U_{fin}$). Substituting equation (3) for equation (5) and solving equation (5) with respect to
 258 t , the knickpoint travel time since the incision rate increase ($t = 0$) is

$$t = \begin{cases} \frac{k_{sn\ ini}}{nU_{ini}} \chi_{kp}(t) & n < 1 \quad (6a) \\ \frac{1}{K} \chi_{kp}(t) & n = 1 \quad (6b) \\ \frac{k_{sn\ fin} - k_{sn\ ini}}{U_{fin} - U_{ini}} \chi_{kp}(t) & n > 1. \quad (6c) \end{cases}$$

260

261 **2.4. Basin-Averaged Erosion Rate Determined from Cosmogenic ^{10}Be Concentration**

262 The ^{10}Be concentration in fluvial sediment (\bar{C} : atoms/g) is used to estimate the average
 263 erosion rate within a catchment (\bar{D} : g/m² yr) (e.g., Brown et al., 1995a; Bierman & Steig, 1996;
 264 Granger et al., 1996) by

$$265 \quad \bar{D} = P_0 \Lambda / \bar{C}, \quad (7)$$

266 where P_0 (atoms/g yr) is the cosmogenic ^{10}Be production rate at the surface and Λ (g/cm²) is the
 267 attenuation length of particles responsible for ^{10}Be production. Because the total sediment mass
 268 produced in a catchment is the sum of the sediment from its nested sub-catchments, average
 269 erosion rates within and outside the sub-catchments can be estimated by analyzing ^{10}Be samples
 270 from multiple sites in the catchment (e.g., Regalla et al., 2013):

$$\bar{D} = \frac{\sum_{i=1}^j D_i A_i}{\sum_{i=1}^j A_i}, \quad (8)$$

where D_i and A_i are the average erosion rate and drainage area of sub-catchment i , respectively, and j is the number of subcatchments.

274

275 **3. Method**

276 **3.1. Observations of Channel and Hillslope Morphology**

277 We compiled observations of the along-trunk variations of channel slope, channel width,
278 and hillslope angle as detailed below. We used the channel slope data to identify the current
279 knickpoint position, and we used the other observations to determine the points where the
280 adjustments of channel width and hillslope angle started and finished.

281

282 **3.1.1. Normalized Steepness Index**

283 We analyzed a digital elevation model (DEM) of the study area to calculate the
284 normalized steepness index k_{sn} every 50 m along trunk streams using Topotoolbox 2
285 (Schwanghart & Scherler, 2014). The DEM, obtained from the Geospatial Information Authority
286 of Japan, has a resolution of 10 m. We first determined A_{crt} and then calculated k_{sn} for channel
287 reaches with $A > A_{crt}$. We also calculated χ (Perron & Royden, 2013) and constructed χ -
288 elevation (z) plots (χ -plots):

$$289 \quad \chi = \int_{x_b}^x (A_0/A(x))^{\frac{m}{n}} dx \quad (9)$$

$$290 \quad z(x) = z(x_b) + (E/KA_0^m)^{\frac{1}{n}} \chi \quad (10)$$

291 where x is the distance along a stream course measured from the outlet of the channel reach, x_b
292 is the distance at the outlet (thus $x_b = 0$). Equation (10) is the integral form of equation (2) under
293 the assumption of a spatially uniform E and K , and it predicts that the slope of a χ -plot
294 represents a reach-averaged value of k_{sn} . A knickpoint appears as a kink in a χ -plot. We used
295 the k_{sn} values and χ -plots to determine the current positions of slope-break knickpoints (at the
296 upstream end of knickzones), where the adjustment of channel slope begins.

297

298 **3.1.2. Field Measurement of Channel Width**

299 We measured bankfull channel widths in the field every 30–100 m along trunk streams
300 using a laser rangefinder (TruPulse 360B Laser Technology). Measurement error is
301 approximately ± 30 cm. Width measurements depend on how one defines flow depth at bankfull
302 stage. The bankfull depth is typically identified based on the limits of active abrasion, vegetation
303 boundaries, and remnants of flood debris (e.g., Whittaker et al., 2007). Where there were
304 multiple candidates for the high-flow depth, we measured channel widths at each candidate level
305 and calculated their average. The measured width of each trunk river was fitted to equation (4) to
306 estimate exponent b based on least squares. We determined b_{ref} by averaging b of all river
307 segments whose width variations were consistent with the general scaling of equation (4). We
308 then used the resulting b_{ref} values and upstream drainage areas calculated from the 10 m DEM
309 to calculate the normalized wideness index k_{wn} .
310

311 **3.1.3. Average Angle of Valley-Side Slopes**

312 We calculated the angles of hillslopes adjacent to trunk streams using the 5 m DEM
313 provided by the Geospatial Information Authority of Japan. We used this high-resolution DEM
314 because the accuracy of hillslope angles depends on the DEM grid size. Because the available 5
315 m DEM lacks data along the streams, we could not use it for the channel analysis. We mapped
316 hillslopes along trunk streams based on the upstream drainage area, slope aspect, and slope
317 curvature. We did not include hillslopes along tributaries with drainage areas greater than A_{crt} as
318 our focus was on trunk streams. Although it was difficult to determine a clear threshold, we also
319 excluded hillslopes along small tributaries (maximum area $< A_{crt}$) visible on the 5 m DEM
320 (Figure S1). We then segmented mapped valley-side slopes every 50 m along trunk streams and
321 calculated average angles for each hillslope segment.
322

323 **3.1.4. Identifying Sections of Transient Response**

324 To identify river sections where hillslopes and channels are undergoing transient
325 response to a knickpoint passage, we calculated 8-point moving averages of k_{wn} and hillslope
326 angle. Given the large natural variability in channel width and hillslope angle, we augmented the
327 moving averages with statistical tests to identify the sections in transience. The Kolmogorov-

328 Smirnov test showed that in Basin 1, k_{wn} values were normally distributed ($p = 0.64$) and
329 hillslope angles were not normally distributed ($p \ll 0.01$) at the 5% significance level.
330 Therefore, we applied the Student's t test for k_{wn} data and the Mann-Whitney U test for hillslope
331 angle data. In these tests, we used 16 contiguous samples and determined whether the difference
332 between the upstream 8 samples and the downstream 8 samples was statistically significant.
333 Despite trying various significance levels, we could not properly identify sections experiencing
334 transient response. Therefore, we defined transient sections as those where the moving average
335 values showed a gradual decrease or increase and where the p -value of statistical tests was
336 smaller than those of adjacent channel sections.

337

338 **3.2. Adjustment Timescales of Channel Width and Hillslope Angle**

339 Using equation (6), we calculated knickpoint travel time for n values of 2/3, 1, and 5/3
340 (e.g., Whipple et al., 2000) and estimated the delay, response, and adjustment times of channel
341 width and valley-side slope angles in response to a sustained increase in incision rates.
342 Normalized channel steepness at the initial and final steady state were defined as the average k_{sn}
343 upstream and downstream of a slope-break knickpoint, respectively. We assumed that the
344 erodibility constant (K) was uniform over time and calculated K using k_{sn} and ^{10}Be -derived
345 erosion rates with equation (3).

346

347 **3.3. Basin-Averaged Erosion Rate Determined from Cosmogenic ^{10}Be Concentration**

348 We collected four sand samples (diameter < 2 mm) from trunk streams and measured
349 ^{10}Be concentrations of quartz grains to determine basin-averaged erosion rates (Figures 1 and
350 S2). We purified quartz following a method adapted from Kohl and Nishiizumi (1992). We first
351 crushed and sieved samples to obtain grains 0.25–1 mm in diameter. These were heated in 9%
352 HCl to remove carbonates, iron oxides, and organic materials, then quartz was separated from
353 the samples using sodium polytungstate. The extracted quartz was leached using a 1% HF and
354 HNO₃ solution to remove residual feldspars and meteoric ^{10}Be . Then, after adding a ^9Be spike,
355 the quartz was dissolved with HF, HNO₃, and HClO₄. After the solution was used in anion- and
356 cation-exchange chromatography, NH₄OH was added, and the precipitant was heated to obtain

357 BeO. $^{10}\text{Be}/^9\text{Be}$ ratios were measured using accelerator mass spectrometry at Micro Analysis
358 Laboratory, Tandem Accelerator, the University of Tokyo (Matsuzaki et al., 2007).

359 ^{10}Be production rates were calculated using scaling factors presented in Stone (2000). We
360 computed topographic shielding factors for all sampled points using the 10 m DEM and an
361 algorithm developed by Li (2013). Attenuation lengths for neutrons, slow muons and fast muons
362 were set at 160, 1500, and 5300 g/cm^2 , respectively (Brown et al., 1995b; Gosse & Phillips,
363 2001; Braucher et al., 2003). Contributions of slow and fast muons to the total ^{10}Be production at
364 the surface were assumed to be 1.2% and 0.65%, respectively (Braucher et al., 2003). We
365 assumed a bulk density of 1.63 g/cm^3 for the shallow subsurface materials on hillslopes
366 (Nakamura et al., 2014). Although it sometimes snows in Iwaki, we did not consider the effect of
367 snow shielding on ^{10}Be production because the snow cover was mostly less than several
368 centimeters deep during 1960–2008 (Japan Meteorological Agency, 2021).

369

370 **4. Results**

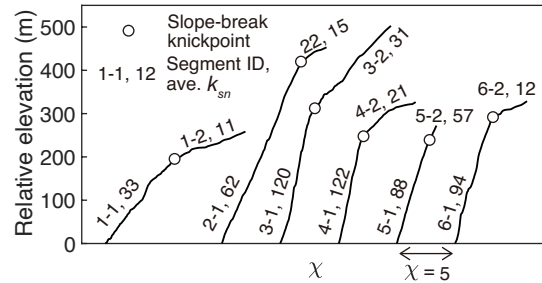
371 **4.1. Channel and Hillslope Morphology**

372 **4.1.1. Steepness of Stream Channels**

373 Calculated values of normalized channel steepness (k_{sn}) are summarized in Figure 3.
374 Each of the six drainage basins contains a slope-break knickpoint dividing the trunk streams into
375 a downstream segment with greater k_{sn} and an upstream segment with smaller k_{sn} (Figures 1
376 and 3). Downstream segments of Basins 2–6 are much steeper than that of Basin 1, suggesting
377 that incision rates in Basin 1 are much slower than in other basins. The channel steepness in the
378 downstream segment of Basin 1 is three times greater than that of the upstream segment (Figure
379 3), suggesting that Basin 1 may be at a transient state. However, because the trunk stream of
380 Basin 1 does not cross the Yunodake fault and we cannot know where the knickpoint formed, we
381 will not discuss its morphological characteristics in detail. A slope-break knickpoint in Basin 3
382 occurs near a boundary between granitic rocks and schist (Figure 1), presenting the possibility
383 that differential rock erodibility may explain the observed increase in k_{sn} . However, channel
384 steepness does not change significantly at similar lithologic boundaries in Basins 3 and 4

385 (Figures 1b and S2). Therefore, we assumed that factors other than differential rock erodibility
 386 contributed to the formation of the knickpoint in Basin 3.

387



388

389 **Figure 3.** A χ -plot for the trunk streams in Basins 1 to 6. Relative elevation (y-axis)

390 denotes the elevation above the basin outlet.

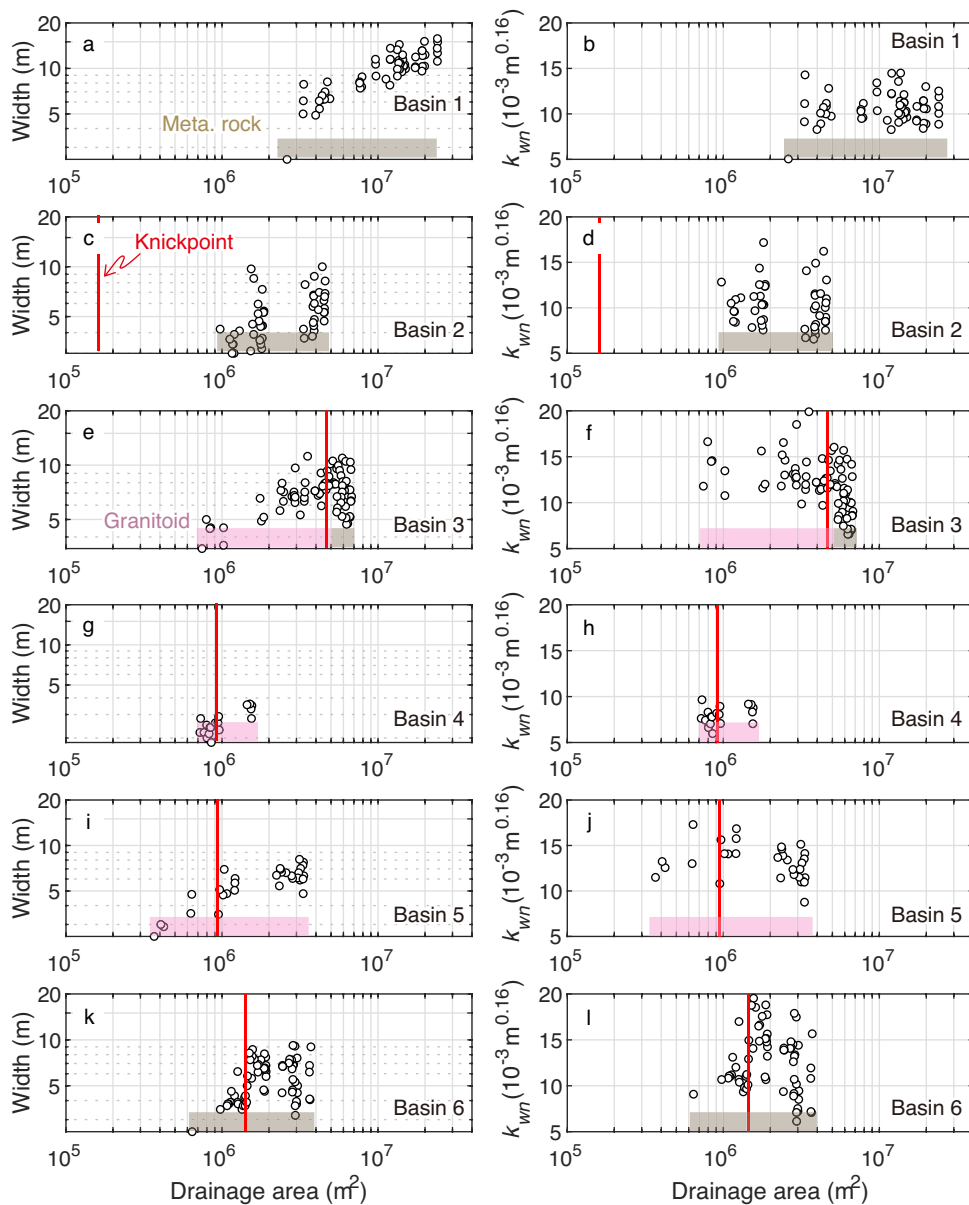
391

392 4.1.2. Channel Width

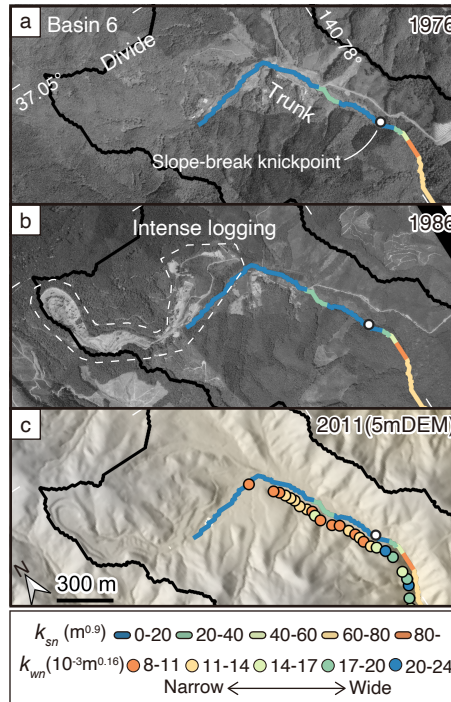
393 We measured channel width and depth at 308 points, which are presented in the
 394 supporting information (Table S2). Channel width in Basins 1, 2, and 4 increases monotonically
 395 with drainage area and follows the general hydraulic scaling of equation (4) (Figure 4; Table 1).
 396 Normalized wideness index (k_{wn} , $b_{ref} = 0.42$) in Basins 1, 2, and 4 do not vary significantly
 397 over their entire reaches (Figure 4). It is noteworthy that k_{wn} for the trunk streams of Basins 1
 398 and 2 are identical despite their twofold difference in k_{sn} . This result implies that their channel
 399 widths are insensitive to changes in channel incision rates or that they have not started to adjust
 400 to the accelerated incision (e.g., Snyder et al., 2003; Zhang et al., 2017).

401 While channel width increases with drainage area in upstream segments of Basins 3 and
 402 5, in their downstream segments channel width decreases or does not change significantly with
 403 increasing drainage area (Figure 4). In Basin 3, channel width starts to decrease at $A = \sim 5.2 \text{ km}^2$,
 404 and that transition occurs near the lithologic boundary between granitoids and metamorphic
 405 rocks (Figures 4e and 4f). These results suggest that substrate property may partly control
 406 channel width. However, the break in the scaling relationship for channel width observed in
 407 Basin 3 cannot be solely attributed to the difference in substrates because the channel width
 408 continues to decrease downstream from the lithologic boundary (Figure 4e and 4f).

409 In Basin 6, the channel width changes by a factor of 2 at $A = 1.5 \text{ km}^2$ (Figure 4k and 4l)
 410 and clearly deviates from the general trend of equation (4). Downstream from this point, bedrock
 411 extensively crops out in the riverbed and channel width decreases with drainage area, which is
 412 likely associated with accelerated river incision as in Basins 3 and 5. The upstream reaches are
 413 covered by thick alluvium. Aerial photographs taken in 1976 and 1986 show that many trees
 414 upstream in Basin 6 were cut during this period and the surrounding areas were widely excavated
 415 (Figure 5). This human activity displaced large amounts of soil, which currently occupies the
 416 channel and results in channel narrowing upstream of the knickpoint.



418 **Figure 4.** (Left) Channel width versus drainage area for the trunk streams. (Right)
 419 Normalized channel wideness ($b_{ref} = 0.42$) versus drainage area. Colored bars at the bottom of
 420 each diagram indicate substrate rock types in the corresponding river sections. Red vertical lines
 421 indicate positions of slope-break knickpoints.



422
 423 **Figure 5.** Deforestation in the headwater area of Basin 6. (a, b) Aerial photographs taken
 424 in 1976 and 1986, respectively. (c) Relief map created from the 5 m DEM issued in 2011 by the
 425 Geospatial Information Authority of Japan. Colored points along the trunk stream show
 426 normalized channel wideness at nearby sites.

427

428 **Table 1**
 429 *Results of Field Measurement and Regression of Channel Width*

430

Basin/ segment	Max. area (km ²)	Min. area (km ²)	k_w	b^*	R^2	Ave k_{wn} ($10^{-3} \text{ m}^{0.16}$)
1	24.1	0.025	3.45	0.43	0.73	10.6
2	4.6	0.021	3.43	0.40	0.41	10.2
3	6.9	0.021	5.37	0.20	0.20	12.0
3-downstream	6.9	6.2	2.52	0.52	0.03	9.2
3-upstream	5.4	0.021	4.70	0.35	0.51	13.2
4	1.6	0.1	2.69	0.52	0.73	8.1
5	3.4	0.4	4.75	0.30	0.64	13.4

5-downstream	3.4	2.8	5.28	0.18	0.00	12.1
5-upstream	2.4	0.4	4.79	<i>0.39</i>	0.65	14.3
6	3.8	0.3	4.73	0.26	0.13	12.8
6-downstream	3.8	1.7	7.19	<i>-0.17</i>	0.03	12.6
6-upstream	1.6	0.3	2.96	1.77	0.53	12.7

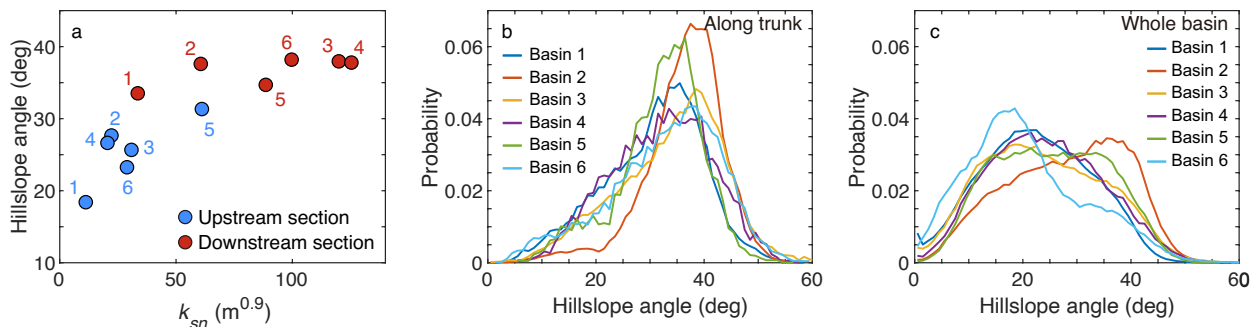
431 *Numbers in italics were used to calculate b_{ref} .

432

433 4.1.3. Angle of Valley-side Slopes

434 As illustrated in Figure 2, hillslopes in Basins 1–6 consist of three sections: an upstream
 435 section with gentler slopes, a downstream section with steeper slopes, and an intervening
 436 transition section. Hillslope angles in the upstream sections were positively correlated with
 437 normalized channel steepness (Figure 6). In the downstream sections, hillslope angles were less
 438 sensitive to channel steepness and clustered at 35° – 38° , suggesting that these are predominantly
 439 threshold hillslopes (e.g., Ouimet et al., 2009). Left-skewed distributions of hillslope angles also
 440 support the interpretation that the downstream sections have threshold hillslopes (Figure 6b)
 441 (DiBiase et al., 2012). These transitions from gentler to steeper hillslopes occur downstream of
 442 the knickpoints and presumably result from the change in incision rates. Also, it is worth noting
 443 that the histograms for hillslope angles along the trunk stream distinctly differ from those for the
 444 whole basin (Figure 6b and 6c).

445



446

447 **Figure 6.** (a) Hillslope angle versus normalized channel steepness for upstream and
 448 downstream segments of the six basins. (b) Histogram of hillslope angles along trunk streams.
 449 (c) Histogram of hillslope angles in each entire basin. The bins in (b) and (c) are 1° wide.

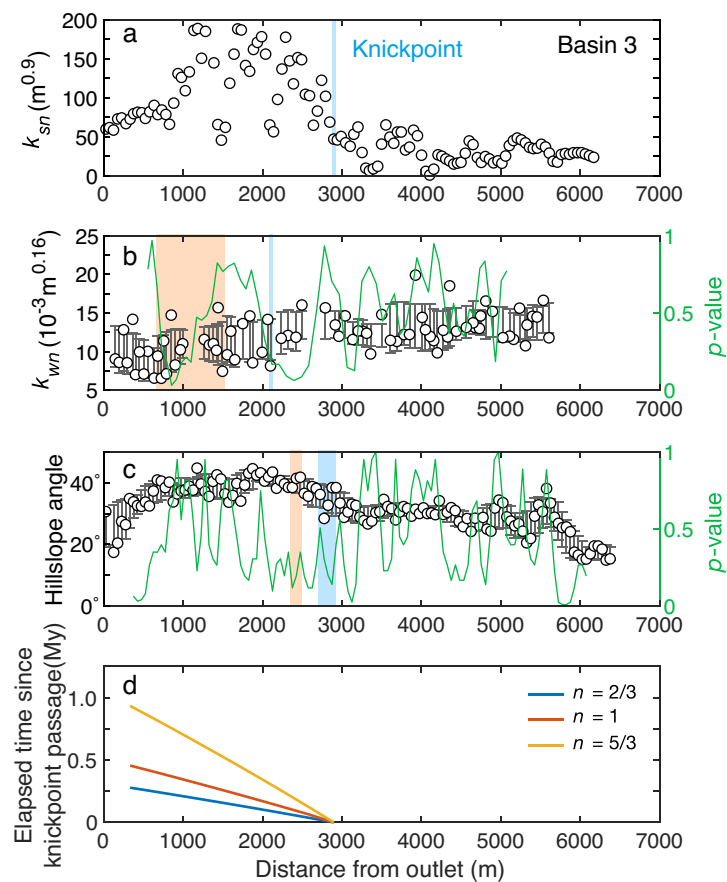
450

451

4.1.4. Identifying Sections undergoing Transient Response

We used the moving averages of channel and hillslope parameters and the p -values from statistical tests to identify river sections experiencing transient response to accelerated incision. Figure 7 shows the along-trunk variations of channel and hillslope morphology in Basin 3, and those for the other basins are shown in Figure S5. As mentioned in section 4.1.1, we excluded Basin 1 from further analysis because its trunk stream does not cross the Yunodake fault. Also, we do not discuss hillslope adjustment time for Basin 5 because the observed increase in hillslope angle starts upstream of the knickpoint.

460



461

Figure 7. Variations of channel width and hillslope morphology along the trunk stream in Basin 3. (a) Normalized channel steepness (k_{sn}). The blue line indicates the current knickpoint position. (b) Normalized channel wideness (k_{wn}). The green line indicates the p -value from Student's t test. (c) Average hillslope angle in each 50 m segment of the trunk stream. The green line indicates the p -value from the Mann-Whitney U test. Gray bars in (b) and (c) represent standard deviation of 8-point moving averages and blue and orange areas indicate sections where

467

468 adjustments start and finish, respectively. (d) Time elapsed since knickpoint passage (knickpoint
469 travel time) for three different values of n .

470

471 **4.2. Substrate Erodibility Calculated from Basin-Averaged Erosion Rates**

472 The basin-averaged erosion rates of our study basins ranged between 260 and 400 g/m²yr,
473 equivalent to 0.16–0.25 mm/yr (Table 2). Basin 4 differs from the others in consisting almost
474 entirely of granitic rock. It also lacks evidence of recent large slope failures, which dilute the
475 average ¹⁰Be concentration of fluvial sand downstream by supplying material with low ¹⁰Be
476 concentrations. Thus, we used equation (8) to calculate the basin-averaged erosion rate of the
477 downstream half of Basin 4 (IWK4-1, Table 2) and found that it is faster than that of the
478 upstream half of Basin 4 (IWK4-2, Table 2). Overall, basin-averaged erosion rates were
479 positively correlated with average k_{sn} (Table 2, Figure S3). Therefore, we assume that the
480 erosion rates determined from the ¹⁰Be concentrations reflect channel incision rates and can be
481 used to calculate the erodibility K in equation (2).

482 Using k_{sn} and basin-averaged erosion rates, we determined the erodibility coefficient K
483 for granitic and metamorphic rocks. These were 1.77×10^{-5} ($n = 2/3$), 4.85×10^{-6} ($n = 1$), and
484 3.70×10^{-7} ($n = 5/3$) m^{0.1}/yr for granitic rocks. To verify these estimates, we calculated erodibility
485 coefficients for similar granitic rocks in the Abukuma massif (Kubo & Yamamoto, 1990) north
486 of the study area using the same DEM and procedure we used in Iwaki (Figure S4; Tables S3,
487 S4). We relied on ¹⁰Be concentrations of fluvial sand reported by Regalla et al. (2013),
488 Nakamura et al. (2014), and Matsushi et al. (2014) to recalculate basin-averaged erosion rates
489 using the same method used in Iwaki. The resulting erodibility coefficients were similar to those
490 obtained in Iwaki: 1.58×10^{-5} ($n = 2/3$), 4.52×10^{-6} ($n = 1$), and 3.90×10^{-7} ($n = 5/3$) m^{0.1}/yr. The
491 coefficients for metamorphic rocks in Iwaki were 1.64×10^{-5} ($n = 2/3$), 5.21×10^{-6} ($n = 1$), and
492 5.30×10^{-7} ($n = 5/3$) m^{0.1}/yr, which were not very different from those for granitic rocks.
493 Although sample limitations may affect the accuracy of the coefficient for metamorphic rocks,
494 considering that the reaches of granitic and metamorphic rocks have comparable channel
495 steepness (Figure 1b), our results indicate that these two rock types have similar erodibility.

496

497 **4.3. Knickpoint Travel Time**

498 To estimate knickpoint travel time, we first calculated uplift (erosion) rates at the initial
 499 and final steady states, using equation (6), based on the standard detachment limited model of
 500 equation (3) (Table 3). Given the erosion rates derived from ^{10}Be data (Table 2), a slope
 501 exponent of $n = 2/3$ yields the most probable estimates of initial and final uplift rates (Table 3).
 502 When calculating knickpoint travel time, we assumed that knickpoints were generated where the
 503 stream intersects the Yunodake fault. The resulting knickpoint travel times were somewhat
 504 similar among Basins 3–6, while the travel time for Basin 1 was much longer than those for the
 505 other basins (Table 4).

506

507 **Table 2**508 *Basin-averaged Erosion Rates Determined from ^{10}Be Concentrations*

Sample ID	Mass sample (g)	Mass ^9Be carrier (g)	$^{10}\text{Be}/^9\text{Be}$ ($\times 10^{-14}$) ^a	^{10}Be concentration (atoms/g)	^{10}Be production rate (atoms/g yr) ^b	Erosion rate (g/m ² /yr)	Erosion rate (mm/yr) ^c	Upstream ave. k_{sn} (m ^{0.9}) ^d
IWK1	26.4364	3.4882	7.5 ± 0.51	55627 ± 4929	7.0 ± 0.4	261 ± 37	0.16 ± 0.03	28
IWK4	39.3525	2.4981	17.5 ± 2.2	67402 ± 9578	6.6 ± 0.4	391 ± 63	0.24 ± 0.04	59
IWK3	39.4954	2.4994	10 ± 0.90	34884 ± 4041	7.2 ± 0.4	405 ± 62	0.25 ± 0.04	25
IWK4-2	40.0002	2.4809	10.6 ± 0.88	36878 ± 3920	6.9 ± 0.4	329 ± 46	0.20 ± 0.03	17
IWK4-1*						444 ± 78	0.28 ± 0.05	90

509 Note. * Average rate for the downstream sub-catchment of Basin 4 calculated from equation (10).

510 ^a Results based on the KNB5-1 ^{10}Be standard (Nishiizumi et al., 2007). The $^{10}\text{Be}/^9\text{Be}$ ratio for the
511 chemical blank was $1.8 \times 10^{-14} \pm 0.30 \times 10^{-14}$.512 ^b We used the production rate at sea level and high latitude of $4.68 \text{ atoms g}^{-1} \text{ yr}^{-1}$, corrected from the
513 value proposed by Stone (2000) assuming a ^{10}Be half-life of 1.387 My (Chmeleff et al., 2010; Korschinek
514 et al., 2010).515 ^c The bulk density of samples was 1.63 g/cm^3 (Nakamura et al., 2014).516 ^d Average k_{sn} for trunk and tributaries upstream from a sampling point.

517

518 **Table 3**519 *Initial and Final Uplift Rates Used to Calculate Knickpoint Travel Time*

Basin	$k_{sn \text{ ini}}$	$k_{sn \text{ fin}}$	$n = 2/3$		$n = 1$		$n = 5/3$	
			U_{ini} (mm/yr)	U_{fin} (mm/yr)	U_{ini} (mm/yr)	U_{fin} (mm/yr)	U_{ini} (mm/yr)	U_{fin} (mm/yr)
2	15.1	61.7	0.10	0.26	0.08	0.32	0.05	0.51

3	31	120	0.17	0.40	0.15	0.63	0.11	1.54
4	20.5	122.4	0.13	0.44	0.10	0.59	0.06	1.12
5	57.2	87.9	0.26	0.35	0.28	0.43	0.31	0.64
6	12	94	0.09	0.37	0.06	0.46	0.02	0.72

520 Note. Uplift rates were calculated using normalized channel steepness and ^{10}Be analyses.

521

522 **Table 4**

523 *Knickpoint Travel Time*

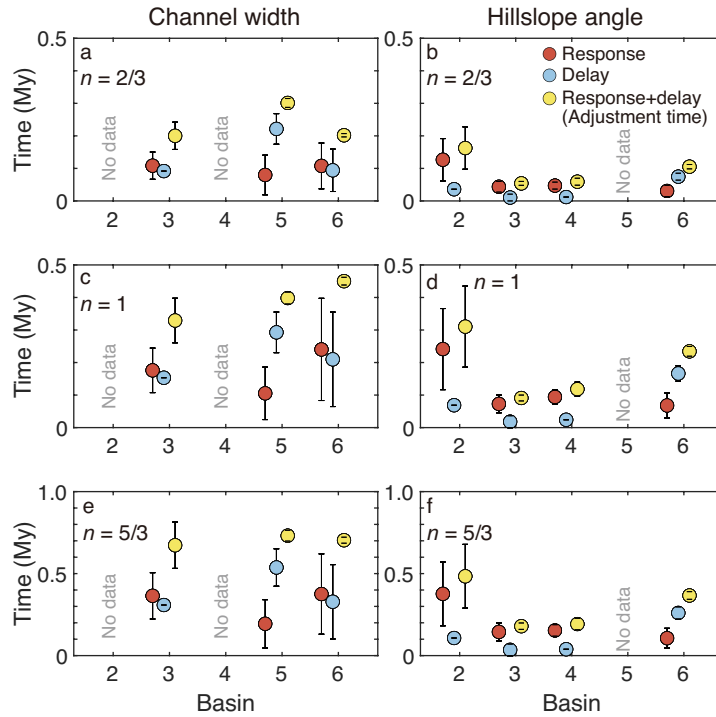
Basin	Knickpoint position (m)	Travel time, $n = 2/3$ (My)	Travel time, $n = 1$ (My)	Travel time, $n = 5/3$ (My)
2	3908	0.73	1.38	2.16
3	2896	0.28	0.45	0.93
4	1154	0.21	0.42	0.69
5	1933	0.40	0.53	0.98
6	2550	0.28	0.62	0.97

524

525 **4.4. Adjustment Timescales**

526 The delay times for hillslope angle ranged between 0 and 0.3 My and were much shorter
 527 than those for channel width (Figure 8). The response times, too, were shorter for hillslope angle
 528 than for channel width. The most preferred case ($n = 2/3$) predicted that the change in hillslope
 529 angle was finished within 5-230 ky after the knickpoint passage. This result is consistent with
 530 response timescales reported in the Oregon Coast Range (Roering et al., 2001) and the Feather
 531 River basin, California (Hurst et al., 2012), which were estimated from sediment transport laws.
 532 The adjustment time for channel width was 2–5 times longer than those of hillslope angles.

533 While it is relatively easy to classify hillslopes into sections based on their degree of
 534 adjustment to the new boundary conditions (Figures 2 and 7), doing the same for channel width
 535 is tricky (Figures 4 and 7). One reason is the large variability in channel width (Figure 4);
 536 another is the large uncertainty in determining when an adjusting channel has achieved the
 537 steady-state form predicted by equation (4). Although we determined that the most downstream
 538 sections in Basins 3, 5, and 6 have adjusted to accelerated incision, it is also possible that our
 539 interpretation is wrong. Therefore, the response and adjustment times of channel width shown in
 540 Figure 8 are minimum estimates.



541

542 **Figure 8.** Delay, response, and adjustment times of channel width (a–c) and hillslope543 angle (d–f) in response to an increase in incision rates for three different values of n .

544

545 **5. Discussion**546 **5.1. Cause of Knickpoint Formation**

547 The common occurrence of slope-break knickpoints and the similar erodibility
 548 coefficients between granitic and metamorphic rocks suggest that incision rates have increased in
 549 the study area. The average erosion rates in Basin 3, which are different upstream and
 550 downstream of the slope-break knickpoint, support the idea that accelerated river incision is
 551 responsible for the observed transient behavior.

552 We interpret the increase in incision rates to the activity of the Yunodake fault because
 553 rivers flowing across the fault (Basins 2–6) are much steeper than the river in Basin 1, away from
 554 the fault (Figure 1). Awata and Kakimi (1985) and Awata (1988) estimated initiation ages of
 555 active faulting in the current stress regime on the Pacific side of Tohoku on the basis of average
 556 slip rates and cumulative displacement. They found that many faults became active after 0.5–1.0
 557 Ma. Doke et al. (2012) conducted an extensive literature review and reached a similar

558 conclusion. Our modeled knickpoint travel times in Iwaki (Table 4) ranged between 0.2 and 0.7
559 My, consistent with the inferred onset of fault activity in Tohoku. Therefore, although there is no
560 direct evidence of the throw rate of the Yunodake fault increasing during the middle Pleistocene,
561 we attribute the generation of slope-break knickpoints to changes in throw rates of the fault.

562

563 **5.2. Implications for Transient Response**

564 The delay and response times of channel width are 2–5 times longer than those of
565 hillslope angle. Depending on the erosion process (the slope exponent n in equation (2)) and the
566 magnitude of the acceleration of river incision, width adjustment can take 0.16–0.81 My after the
567 knickpoint passage (Figure 8). In addition, our observations confirmed that the transient response
568 takes place at different spatiotemporal scales for channel slope, channel width, and hillslope
569 angle. Thus channel width and hillslope angle may be continuing to adjust even when the river
570 lacks a prominent knickpoint. Since channel characteristics and hillslope morphology are the
571 primary controls of river incision (e.g., Whipple & Tucker, 2002), correctly identifying the
572 adjusted sections within a catchment is essential for assessing the transient response to an
573 increase in incision rates.

574 Another inference from our observation is on the transient response of channel width.
575 The ratio of sediment supply to transport capacity dictates the dynamics of channel width
576 adjustment (e.g., Finnegan et al., 2007; Yanites & Tucker, 2010; Baynes et al., 2020). Because
577 the total sediment supply into a channel is modulated by the form of upstream hillslopes (e.g.,
578 Roering et al., 2007), the adjustment of channel width is expected to continue until a slope-break
579 knickpoint reaches the headwaters and adjacent hillslopes achieve their steady-state forms.
580 However, despite the fact that most hillslopes exhibit pre-adjustment forms in Basins 3, 5, and 6
581 (Figures 6b and 6c), the channel widths in their downstream sections appear to be adjusted to the
582 accelerated incision (Figures 4 and S5, Table S4). It appears, then, that the dynamics of width
583 adjustment are not simply a response to the increase in total sediment supply from upstream.

584 An alternative interpretation is that the channel width adjustment has not in fact been
585 completed, and the ongoing changes in the channel are too small to be confidently detected due
586 to measurement error and natural variability. This interpretation is compatible with the result of
587 numerical modeling, which predicts that the response of channel width is rapid at first, then

588 decays as the response progresses (Yanites, 2018). We speculate that this gradual decrease is
589 related to the downstream fining of sediment. Abrasion and selective transport are the main
590 drivers of downstream fining (i.e., mass reduction) of sediment (e.g., Parker, 1991). Their effects
591 typically scale with travel distance and can be significant even after only a few kilometers of
592 transport (e.g., Parker, 1991; Phillips & Jerolmack, 2014; Miller et al., 2014). Therefore, the rate
593 of increase in sediment supply at a point downstream should slow as the knickpoint travels
594 upstream, as demonstrated by numerical experiments (Yanites, 2018). Given the dependence of
595 channel width on grain size and the ratio of sediment supply to transport capacity (e.g., Yanites
596 & Tucker, 2010; Finnegan et al., 2017), we attribute the decay in the response speed of channel
597 width to a decline in the rate of increase in sediment supply.

598

599 **5.3. Timescale of Catchment-Scale Adjustment**

600 The adjustment of an entire catchment is a more complex matter than the adjustment of a
601 trunk stream. Knickpoint travel speed depends on stream discharge (e.g., Whipple & Tucker,
602 1999; Hayakawa & Matsukura, 2003; Bishop et al., 2005), and the travel time from its origin to
603 the channel head is on the order of 10^5 – 10^6 years (Whipple, 2001; Whittaker and Boulton, 2012).
604 The adjustment of channel slopes in tributaries must also be considered; this is sometimes
605 prolonged where hanging valleys are present (Wobus et al., 2006b; Crosby et al., 2007; DiBiase
606 et al., 2015). Adjustments of channel width and hillslope require hundreds of thousands more
607 years after a knickpoint has finished propagating to the heads of the trunk and tributaries.
608 Moreover, other aspects of channels and hillslopes respond to changes in channel incision rates,
609 such as channel sinuosity (Turowski, 2018) and hilltop curvature (Gabet et al., 2021).
610 Morphological adjustments of these variables are also triggered by climate variability and occur
611 at timescales of 10^5 – 10^6 years (e.g., Whipple, 2001), although fluvial systems might not fully
612 adjust to high-frequency climatic oscillations such as Milankovitch cycles (Armitage et al., 2013;
613 Goren, 2016). Given all these factors, it is clear that catchment-scale adjustment to accelerated
614 incision takes much longer than the knickpoint travel time within the trunk stream. This further
615 confirms that to estimate rates of erosion or base-level fall, one must consider whether the river
616 system has reached a steady state even when it contains no prominent knickpoint.

617

618 **6. Conclusions**

619 Based on the observed channel and hillslope geometries and knickpoint travel time, we
620 have estimated their adjustment times to accelerated incision. Our approach enables us to
621 estimate both delay and response times of channel width and hillslope angles, which are
622 otherwise difficult to constrain in an actual landscape. Our results indicate that hillslope
623 adjustment starts and finishes much earlier than channel width adjustment. Change in hillslope
624 angle starts soon after the passage of a knickpoint (10^0 – 10^4 yr) and generally finishes on the
625 order of 10^5 years later. Channel width adjustment takes 2–5 times longer than hillslope
626 adjustment. Unlike hillslope angle, channel width has adjustment times that are not always
627 negligible compared to that of channel slope, which depends closely on knickpoint travel time.

628 The longevity of catchment-scale adjustment time and the different adjustment timescales
629 among channel slope, channel width, and hillslope angles remind us that we need to infer erosion
630 or uplift rates from channel reaches that are in a well-defined steady state. Our findings also
631 suggest that it is important to understand the temporal evolution of erosion rates during the
632 adjustment of individual channel and hillslope components. Lastly, it has to be noted that our
633 estimates of knickpoint travel time do not explicitly consider important factors including the
634 effects of sediment characteristics and temporal changes in precipitation. Because these factors
635 may significantly alter estimates of adjustment time, inter-model comparisons or more
636 sophisticated models of migrating knickpoints are necessary to better understand the transient
637 response of bedrock rivers.

638

639 **Acknowledgments**

640 We thank Chia-Yu Chen (National Taiwan University) for helpful comments and A.
641 Morikawa, K. Kitamura (Kyoto University), N. Miyauchi, and Y. Tsuchiya (The University of
642 Tokyo) for their assistance during preparation of the ^{10}Be samples. This work was supported by
643 the International Joint Graduate Program in Earth and Environmental Sciences, Tohoku
644 University. N. Takahashi and R. Ohta thank the staff at Yunodake sanso in Iwaki for their
645 generous support during our fieldwork. We obtained DEM data from the Geospatial Authority of
646 Japan and NOAA (ETOPO1). Some color maps were obtained from Cramer (2018).

647

648 **References**

- 649 Ahnert, F. (1970). Functional relationships between denudation, relief, and uplift in large mid-
650 latitude drainage basins. *American Journal of science*, 268, 243–263.
651 <https://doi.org/10.2475/ajs.268.3.243>
- 652 Allen, G. H., Barnes, J. B., Pavelsky, T. M., & Kirby, E. (2013). Lithologic and tectonic controls
653 on bedrock channel form at the northwest Himalayan front. *Journal of Geophysical
654 Research: Earth Surface*, 118(3), 1806–1825. <https://doi.org/10.1002/jgrf.20113>
- 655 Armitage, J. J., Dunkley Jones, T., Duller, R. A., Whittaker, A. C., & Allen, P. A. (2013).
656 Temporal buffering of climate-driven sediment flux cycles by transient catchment
657 response. *Earth and Planetary Science Letters*, 369–370, 200–210.
658 <https://doi.org/10.1016/j.epsl.2013.03.020>
- 659 Awata, Y. (1988). Shortening of the central inner arc of the northeast Japan and movement of the
660 Pacific plate. *Chikyu Monthly*, 10(9), 586–591.
- 661 Awata, Y., & Kakimi, T. (1985). Quaternary tectonics and damaging earthquakes in northeast
662 Honshu, Japan. *Earthquake Prediction Research*, 3, 231–251.
- 663 Baynes, E. R. C., Lague, D., Steer, P., Bonnet, S., & Illien, L. (2020). Sediment flux-driven
664 channel geometry adjustment of bedrock and mixed gravel–bedrock rivers. *Earth Surface
665 Processes and Landforms*, 45(14), 3714–3731. <https://doi.org/10.1002/esp.4996>
- 666 Baynes, E. R. C., Lague, D., Steer, P., & Davy, P. (2022). Dynamic bedrock channel width
667 during knickpoint retreat enhances undercutting of coupled hillslopes. *Earth Surface
668 Processes and Landforms*. <https://doi.org/10.1002/esp.5477>
- 669 Bierman, P., & Steig, E. J. (1996). Estimating rates of denudation using cosmogenic isotope
670 abundances in sediment. *Earth Surface Processes and Landforms*, 21(2), 125–139.
671 [https://doi.org/10.1002/\(sici\)1096-9837\(199602\)21:2<125::aid-esp511>3.0.co;2-8](https://doi.org/10.1002/(sici)1096-9837(199602)21:2<125::aid-esp511>3.0.co;2-8)
- 672 Bishop, P., Hoey, T. B., Jansen, J. D., & Lexartza Artza, I. (2005). Knickpoint recession rate and
673 catchment area: The case of uplifted rivers in eastern Scotland. *Earth Surface Processes
674 and Landforms*, 30(6), 767–778. <https://doi.org/10.1002/esp.1191>
- 675 Braucher, R., Brown, E. T., Bourlès, D. L., & Colin, F. (2003). In situ produced ¹⁰Be measurements at great depths:
676 Implications for production rates by fast muons. *Earth and Planetary Science Letters*,
677 211(3–4), 251–258. [https://doi.org/10.1016/S0012-821X\(03\)00205-X](https://doi.org/10.1016/S0012-821X(03)00205-X)
- 678 Brown, E. T., Stallard, R. F., Larsen, M. C., Raisbeck, G. M., & Yiou, F. (1995a). Denudation

- 679 rates determined from the accumulation of in situ-produced ^{10}Be in the luquillo
680 experimental forest, Puerto Rico. *Earth and Planetary Science Letters*, 129(1–4), 193–202.
681 [https://doi.org/10.1016/0012-821X\(94\)00249-X](https://doi.org/10.1016/0012-821X(94)00249-X)
- 682 Brown, E. T., Bourlès, D. L., Colin, F., Raisbeck, G. M., Yiou, F., & Desgarceaux, S. (1995b).
683 Evidence for muon-induced production of ^{10}Be in near-surface rocks from the Congo.
684 *Geophysical Research Letters*, 22(6), 703–706. <https://doi.org/10.1029/95GL00167>
- 685 Chen, Y. W., Shyu, J. B. H., & Chang, C. P. (2015). Neotectonic characteristics along the eastern
686 flank of the Central Range in the active Taiwan orogen inferred from fluvial channel
687 morphology. *Tectonics*, 34(10), 2249–2270. <https://doi.org/10.1002/2014TC003795>
- 688 Chmeleff, J., von Blanckenburg, F., Kossert, K., & Jakob, D. (2010). Determination of the ^{10}Be
689 half-life by multicollector ICP-MS and liquid scintillation counting. *Nuclear Instruments*
690 *and Methods in Physics Research, Section B: Beam Interactions with Materials and Atoms*,
691 268(2), 192–199. <https://doi.org/10.1016/j.nimb.2009.09.012>
- 692 Crameri, F. (2018). Scientific colour maps (Version 7.0.0). *Zenodo*.
693 <https://doi.org/10.5281/ZENODO.1243862>
- 694 Crosby, B. T., & Whipple, K. X. (2006). Knickpoint initiation and distribution within fluvial
695 networks: 236 waterfalls in the Waipaoa River, North Island, New Zealand.
696 *Geomorphology*, 82(1–2), 16–38. <https://doi.org/10.1016/j.geomorph.2005.08.023>
- 697 Crosby, B. T., Whipple, K. X., Gasparini, N. M., & Wobus, C. W. (2007). Formation of fluvial
698 hanging valleys: Theory and simulation. *Journal of Geophysical Research*, 112(F3),
699 F03S10. <https://doi.org/10.1029/2006JF000566>
- 700 DiBiase, R. A., Heimsath, A. M., & Whipple, K. X. (2012). Hillslope response to tectonic
701 forcing in threshold landscapes. *Earth Surface Processes and Landforms*, 37(8), 855–865.
702 <https://doi.org/10.1002/esp.3205>
- 703 DiBiase, R. A., Whipple, K. X., Lamb, M. P., & Heimsath, A. M. (2015). The role of waterfalls
704 and knickzones in controlling the style and pace of landscape adjustment in the western
705 San Gabriel Mountains, California. *Bulletin of the Geological Society of America*, 127(3–
706 4), 539–559. <https://doi.org/10.1130/B31113.1>
- 707 Doke, R., Tanikawa, S., Yasue, K., Nakayasu, A., Niizato, T., Umeda, K., & Tanaka, T. (2012).
708 Spatial patterns of initiation ages of active faulting in the Japanese islands. *Active Fault*
709 *Research*, 37, 1–15. https://doi.org/10.11462/afr.2012.37_1

- 710 Finnegan, N. J., Sklar, L. S., & Fuller, T. K. (2007). Interplay of sediment supply, river incision,
711 and channel morphology revealed by the transient evolution of an experimental bedrock
712 channel. *Journal of Geophysical Research: Earth Surface*, 112(3), 1–17.
713 <https://doi.org/10.1029/2006JF000569>
- 714 Finnegan, N. J., Klier, R. A., Johnstone, S., Pfeiffer, A. M., & Johnson, K. (2017). Field
715 evidence for the control of grain size and sediment supply on steady-state bedrock river
716 channel slopes in a tectonically active setting. *Earth Surface Processes and Landforms*,
717 42(14), 2338–2349. <https://doi.org/10.1002/esp.4187>
- 718 Flint, J. J. (1974). Stream gradient as a function of order, magnitude, and discharge. *Water*
719 *Resources Research*, 10(5), 969–973. <https://doi.org/10.1029/WR010i005p00969>
- 720 Fukushima, Y., Takada, Y., & Hashimoto, M. (2013). Complex ruptures of the 11 April 2011
721 Mw 6.6 Iwaki earthquake triggered by the 11 March 2011 Mw 9.0 Tohoku earthquake,
722 Japan. *Bulletin of the Seismological Society of America*, 103(2 B), 1572–1583.
723 <https://doi.org/10.1785/0120120140>
- 724 Gabet, E. J., Mudd, S. M., Wood, R. W., Grieve, S. W. D., Binnie, S. A., & Dunai, T. J. (2021).
725 Hilltop curvature increases with the square root of erosion rate. *Journal of Geophysical*
726 *Research: Earth Surface*, 126(5), 1–16. <https://doi.org/10.1029/2020jf005858>
- 727 Gallen, S. F., & Wegmann, K. W. (2017). River profile response to normal fault growth and
728 linkage: An example from the Hellenic forearc of south-central Crete, Greece. *Earth*
729 *Surface Dynamics*, 5(1), 161–186. <https://doi.org/10.5194/esurf-5-161-2017>
- 730 Geological Survey of Japan, 2020. Seamless Digital Geological Map of Japan. Geological
731 Survey of Japan. Retrieved from <https://gbank.gsj.jp/seamless/v2.html>
- 732 Goren, L. (2016). A theoretical model for fluvial channel response time during time-dependent
733 climatic and tectonic forcing and its inverse applications. *Geophysical Research Letters*,
734 43(20), 10,753–10,763. <https://doi.org/10.1002/2016GL070451>
- 735 Gosse, J. C., & Phillips, F. M. (2001). Terrestrial in situ cosmogenic nuclides: Theory and
736 application. *Quaternary Science Reviews*, 20(14), 1475–1560.
737 [https://doi.org/10.1016/S0277-3791\(00\)00171-2](https://doi.org/10.1016/S0277-3791(00)00171-2)
- 738 Granger, D. E., Kirchner, J. W., & Finkel, R. (1996). Spatially averaged long-term erosion rates
739 measured from in situ-produced cosmogenic nuclides in alluvial sediment. *Journal of*
740 *Geology*, 104(3), 249–257. <https://doi.org/10.1086/629823>

- 741 Hayakawa, Y., & Matsukura, Y. (2003). Recession rates of waterfalls in Boso Peninsula, Japan,
742 and a predictive equation. *Earth Surface Processes and Landforms*, 28(6), 675–684.
743 <https://doi.org/10.1002/esp.519>
- 744 Hiroi, Y., Yokose, M., Oba, T., Kishi, S., Nohara, T., & Yao, A. (1987). Discovery of Jurassic
745 radiolaria from acmite-rhodonite-bearing metachert of the Gosaisyo metamorphic rocks in
746 the Abukuma terrane, northeastern Japan. *Journal of the Geological Society of Japan*,
747 93(6), 445–448. <https://doi.org/10.5575/geosoc.93.445>
- 748 Howard, A. D., & Kerby, G. (1983). Channel changes in badlands. *Geological Society of*
749 *America Bulletin*, 94(6), 739–752. [https://doi.org/10.1130/0016-
750 *7606\(1983\)94<739:CCIB>2.0.CO;2*](https://doi.org/10.1130/0016-7606(1983)94<739:CCIB>2.0.CO;2)
- 751 Hurst, M. D., Mudd, S. M., Walcott, R., Attal, M., & Yoo, K. (2012). Using hilltop curvature to
752 derive the spatial distribution of erosion rates. *Journal of Geophysical Research: Earth*
753 *Surface*, 117(F2), F02017. <https://doi.org/10.1029/2011JF002057>
- 754 Imanishi, K., Ando, R., & Kuwahara, Y. (2012). Unusual shallow normal-faulting earthquake
755 sequence in compressional northeast Japan activated after the 2011 off the Pacific coast of
756 Tohoku earthquake. *Geophysical Research Letters*, 39(9), L09306.
757 <https://doi.org/10.1029/2012GL051491>
- 758 Japan Meteorological Agency (2021). Past meteorological data.
759 <http://www.data.jma.go.jp/obd/stats/etrn/index.php> (accessed 27 April, 2021)
- 760 Kano, H., Kuroda, Y., Uruno, K., Nureki, T., Kanisawa, S., Maruyama, T., Umemura, H.,
761 Matsukawa, H., Seto, N., Ohira, Y., Sato, S., & Isshiki, N. (1973). Geology of the
762 Takanuki district (07-70, scale 1:50,000). Tsukuba: Geological Survey of Japan. Kirby, E.,
763 & Whipple, K. X. (2012). Expression of active tectonics in erosional landscapes. *Journal*
764 *of Structural Geology*, 44, 54–75. <https://doi.org/10.1016/j.jsg.2012.07.009>
- 765 Kohl, C., & Nishiizumi, K. (1992). Chemical isolation of quartz for measurement of in-situ-
766 produced cosmogenic nuclides. *Geochimica et Cosmochimica Acta*, 56(9), 3583–3587.
767 [https://doi.org/10.1016/0016-7037\(92\)90401-4](https://doi.org/10.1016/0016-7037(92)90401-4)
- 768 Korschinek, G., Bergmaier, A., Faestermann, T., Gerstmann, U. C., Knie, K., Rugel, G., et al.
769 (2010). A new value for the half-life of ^{10}Be by Heavy-Ion Elastic Recoil Detection and
770 liquid scintillation counting. *Nuclear Instruments and Methods in Physics Research,*
771 *Section B: Beam Interactions with Materials and Atoms*, 268(2), 187–191.

- 772 <https://doi.org/10.1016/j.nimb.2009.09.020>
- 773 Kubo, K., & Yamamoto, T. (1990). Cretaceous intrusive rocks of the Haramachi district, eastern
774 margin of the Abukuma mountains. *Journal of Geological Society of Japan*, 96(9), 731–
775 743. <https://doi.org/10.5575/geosoc.96.731>
- 776 Kubo, K., Yanagisawa, Y., Yamamoto, T., Nakae, S., Takahashi, Y., Toshimitsu, S., Banno, Y.,
777 Miyachi, Y., Takahashi, M., Komazawa, M., & Ohno, T. (2007). Geological map of Japan,
778 Shirakawa (NJ54-17-23, scale 1:200,000). Tsukuba: Geological Survey of Japan.
- 779 Lavé, J., & Avouac, J. P. (2001). Fluvial incision and tectonic uplift across the Himalayas of
780 central Nepal. *Journal of Geophysical Research: Solid Earth*, 106(B11), 26561–26591.
781 <https://doi.org/10.1029/2001jb000359>
- 782 Li, Y.-k. (2013). Determining topographic shielding from digital elevation models for
783 cosmogenic nuclide analysis: A GIS approach and field validation. *Journal of Mountain*
784 *Science*, 10(3), 355–362. <https://doi.org/10.1007/s11629-013-2564-1>
- 785 Matsushi, Y., Matsuzaki, H., & Makino, H. (2014). Testing models of landform evolution by
786 determining the denudation rates of mountains watersheds using terrestrial cosmogenic
787 nuclides. *Transactions, Japanese Geomorphological Union*, 35(2), 165–185.
- 788 Matsuzaki, H., Nakano, C., Tsuchiya, Y. (Sunohara), Kato, K., Maejima, Y., Miyairi, Y., et al.
789 (2007). Multi-nuclide AMS performances at MALT. *Nuclear Instruments and Methods in*
790 *Physics Research, Section B: Beam Interactions with Materials and Atoms*, 259(1), 36–40.
791 <https://doi.org/10.1016/j.nimb.2007.01.145>
- 792 Miller, K. L., Szabó, T., Jerolmack, D. J., & Domokos, G. (2014). Quantifying the significance
793 of abrasion and selective transport for downstream fluvial grain size evolution. *Journal of*
794 *Geophysical Research: Earth Surface*, 119(11), 2412–2429.
795 <https://doi.org/10.1002/2014JF003156>
- 796 Mitchell, N. A., & Yanites, B. J. (2019). Spatially variable increase in rock uplift in the northern
797 U.S. Cordillera recorded in the distribution of river knickpoints and incision depths.
798 *Journal of Geophysical Research: Earth Surface*, 124(5), 1238–1260.
799 <https://doi.org/10.1029/2018JF004880>
- 800 Mitsui, S. (1971). Studies on the mechanism of deformation of sedimentary rocks in the Iwaki
801 area of the Joban Coal-Field, Fukushima Prefecture. *The science reports of the Tohoku*
802 *University. Second series, Geology*, 42, 199–272. <http://hdl.handle.net/10097/28814>

- 803 Miyashita, Y. (2018). Holocene paleoseismic history of the Yunodake fault ruptured by the 2011
804 Fukushima-ken Hamadori earthquake, Fukushima Prefecture, Japan. *Geomorphology*, 323,
805 70–79. <https://doi.org/10.1016/j.geomorph.2018.08.040>
- 806 Montgomery, D. R., & Brandon, M. T. (2002). Topographic controls on erosion rates in
807 tectonically active mountain ranges. *Earth and Planetary Science Letters*, 201(3–4), 481–
808 489. [https://doi.org/10.1016/S0012-821X\(02\)00725-2](https://doi.org/10.1016/S0012-821X(02)00725-2)
- 809 Montgomery, D. R., & Foufoula-Georgiou, E. (1993). Channel network source representation
810 using digital elevation models. *Water Resources Research*, 29(12), 3925–3934.
811 <https://doi.org/10.1029/93WR02463>
- 812 Montgomery, D. R., & Gran, K. B. (2001). Downstream variations in the width of bedrock
813 channels. *Water Resources Research*, 37(6), 1841–1846.
814 <https://doi.org/10.1029/2000WR900393>
- 815 Mudd, S. M., & Furbish, D. J. (2007). Responses of soil-mantled hillslopes to transient channel
816 incision rates. *Journal of Geophysical Research: Earth Surface*, 112(3), 1–12.
817 <https://doi.org/10.1029/2006JF000516>
- 818 Nakamura, A., Yokoyama, Y., Shiroya, K., Miyairi, Y., & Matsuzaki, H. (2014). Direct
819 comparison of site-specific and basin-scale denudation rate estimation by in situ
820 cosmogenic nuclides: An example from the Abukuma Mountains, Japan. *Progress in Earth
821 and Planetary Science*, 1(1), 1–11. <https://doi.org/10.1186/2197-4284-1-9>
- 822 Nakata, T., & Imaizumi, T. (Eds.) (2002). Digital active fault map of Japan. Tokyo: University
823 of Tokyo press.
- 824 Nishiizumi, K., Imamura, M., Caffee, M. W., Southon, J. R., Finkel, R. C., & McAninch, J.
825 (2007). Absolute calibration of ^{10}Be AMS standards. *Nuclear Instruments and Methods in
826 Physics Research, Section B: Beam Interactions with Materials and Atoms*, 258(2), 403–
827 413. <https://doi.org/10.1016/j.nimb.2007.01.297>
- 828 Ouimet, W. B., Whipple, K. X., & Granger, D. E. (2009). Beyond threshold hillslopes: Channel
829 adjustment to base-level fall in tectonically active mountain ranges. *Geology*, 37(7), 579–
830 582. <https://doi.org/10.1130/G30013A.1>
- 831 Parker, G. (1991). Selective sorting and abrasion of river gravel. I: Theory. *Journal of Hydraulic
832 Engineering*, 117(2), 131–147. [https://doi.org/10.1061/\(ASCE\)0733-
833 9429\(1991\)117:2\(131\)](https://doi.org/10.1061/(ASCE)0733-9429(1991)117:2(131))

- 834 Perron, J. T., & Royden, L. (2013). An integral approach to bedrock river profile analysis. *Earth*
835 *Surface Processes and Landforms*, 38(6), 570–576. <https://doi.org/10.1002/esp.3302>
- 836 Phillips, C. B., & Jerolmack, D. J. (2014). Dynamics and mechanics of bed-load tracer particles.
837 *Earth Surface Dynamics*, 2(2), 513–530. <https://doi.org/10.5194/esurf-2-513-2014>
- 838 Regalla, C., Kirby, E., Fisher, D., & Bierman, P. (2013). Active forearc shortening in Tohoku,
839 Japan: Constraints on fault geometry from erosion rates and fluvial longitudinal profiles.
840 *Geomorphology*, 195, 84–98. <https://doi.org/10.1016/j.geomorph.2013.04.029>
- 841 Reinhardt, L. J., Bishop, P., Hoey, T. B., Dempster, T. J., & Sanderson, D. C. W. (2007).
842 Quantification of the transient response to base-level fall in a small mountain catchment:
843 Sierra Nevada, southern Spain. *Journal of Geophysical Research*, 112(F3), F03S05.
844 <https://doi.org/10.1029/2006JF000524>
- 845 Roering, J. J. (2008). How well can hillslope evolution models “explain” topography?
846 Simulating soil transport and production with high-resolution topographic data. *Bulletin of*
847 *the Geological Society of America*, 120(9–10), 1248–1262.
848 <https://doi.org/10.1130/B26283.1>
- 849 Roering, J. J., Kirchner, J. W., & Dietrich, W. E. (2001). Hillslope evolution by nonlinear, slope-
850 dependent transport: Steady state morphology and equilibrium adjustment timescales.
851 *Journal of Geophysical Research: Solid Earth*, 106(B8), 16499–16513.
852 <https://doi.org/10.1029/2001jb000323>
- 853 Roering, J. J., Perron, J. T., & Kirchner, J. W. (2007). Functional relationships between
854 denudation and hillslope form and relief. *Earth and Planetary Science Letters*, 264(1–2),
855 245–258. <https://doi.org/10.1016/j.epsl.2007.09.035>
- 856 Royden, L., & Perron, J. T. (2013). Solutions of the stream power equation and application to the
857 evolution of river longitudinal profiles. *Journal of Geophysical Research: Earth Surface*,
858 118(2), 497–518. <https://doi.org/10.1002/jgrf.20031>
- 859 Schwanghart, W., & Scherler, D. (2014). Short Communication: TopoToolbox 2 - MATLAB-
860 based software for topographic analysis and modeling in Earth surface sciences. *Earth*
861 *Surface Dynamics*, 2(1), 1–7. <https://doi.org/10.5194/esurf-2-1-2014>
- 862 Snyder, N. P., Whipple, K. X., Tucker, G. E., & Merritts, D. J. (2000). Landscape response to
863 tectonic forcing: Digital elevation model analysis of stream profiles in the Mendocino
864 triple junction region, Northern California. *Bulletin of the Geological Society of America*,

- 865 112(8), 1250–1263. <https://doi.org/10.1130/0016->
866 [7606\(2000\)112<1250:LRTTFD>2.0.CO;2](https://doi.org/10.1130/0016-7606(2000)112<1250:LRTTFD>2.0.CO;2)
- 867 Snyder, N. P., Whipple, K. X., Tucker, G. E., & Merritts, D. J. (2003). Channel response to
868 tectonic forcing: Field analysis of stream morphology and hydrology in the Mendocino
869 triple junction region, northern California. *Geomorphology*, 53(1–2), 97–127.
870 [https://doi.org/10.1016/S0169-555X\(02\)00349-5](https://doi.org/10.1016/S0169-555X(02)00349-5)
- 871 Stock, J., & Dietrich, W. E. (2003). Valley incision by debris flows: Evidence of a topographic
872 signature. *Water Resources Research*, 39(4), 1089.
873 <https://doi.org/10.1029/2001WR001057>
- 874 Stone, J. O. (2000). Air pressure and cosmogenic isotope production. *Journal of Geophysical*
875 *Research*, 105(B10), 23753–23759. <https://doi.org/10.1029/2000jb900181>
- 876 Toda, S., & Tsutsumi, H. (2013). Simultaneous reactivation of two, subparallel, inland normal
877 faults during the Mw 6.6 11 April 2011 Iwaki earthquake triggered by the M w 9.0
878 Tohoku-oki, Japan, Earthquake. *Bulletin of the Seismological Society of America*, 103(2
879 B), 1584–1602. <https://doi.org/10.1785/0120120281>
- 880 Turowski, J. M. (2018). Alluvial cover controlling the width, slope and sinuosity of bedrock
881 channels. *Earth Surface Dynamics*, 6(1), 29–48. <https://doi.org/10.5194/esurf-6-29-2018>
- 882 Turowski, J. M. (2020). Mass balance, grade, and adjustment timescales in bedrock channels.
883 *Earth Surface Dynamics*, 8(1), 103–122. <https://doi.org/10.5194/esurf-8-103-2020>
- 884 Whipple, K. X. (2001). Fluvial Landscape Response Time: How Plausible Is Steady-State
885 Denudation? *American Journal of Science*, 301(4–5), 313–325.
886 <https://doi.org/10.2475/ajs.301.4-5.313>
- 887 Whipple, K. X. (2004). Bedrock rivers and the geomorphology of active orogens. *Annual Review*
888 *of Earth and Planetary Sciences*, 32(1), 151–185.
889 <https://doi.org/10.1146/annurev.earth.32.101802.120356>
- 890 Whipple, K. X., & Tucker, G. E. (1999). Dynamics of the stream-power river incision model:
891 Implications for height limits of mountain ranges, landscape response timescales, and
892 research needs. *Journal of Geophysical Research: Solid Earth*, 104(B8), 17661–17674.
893 <https://doi.org/10.1029/1999jb900120>
- 894 Whipple, K. X., & Tucker, G. E. (2002). Implications of sediment-flux-dependent river incision
895 models for landscape evolution. *Journal of Geophysical Research*, 107(B2), 2039.

- 896 <https://doi.org/10.1029/2000jb000044>
- 897 Whipple, K. X., Hancock, G. S., & Anderson, R. S. (2000). River incision into bedrock:
898 Mechanics and relative efficacy of plucking, abrasion, and cavitation. *Bulletin of the*
899 *Geological Society of America*, 112(3), 490–503. [https://doi.org/10.1130/0016-](https://doi.org/10.1130/0016-7606(2000)112<490:RIIBMA>2.0.CO;2)
900 [7606\(2000\)112<490:RIIBMA>2.0.CO;2](https://doi.org/10.1130/0016-7606(2000)112<490:RIIBMA>2.0.CO;2)
- 901 Whipple, K. X., DiBiase, R. A., & Crosby, B. T. (2013). Bedrock rivers. In Shroder, J. (Editor in
902 Chief), Wohl, E. (Ed.), *Treatise on Geomorphology* (Vol. 9, pp. 550–573). San Diego, CA:
903 Academic Press. <https://doi.org/10.1016/B978-0-12-374739-6.00254-2>
- 904 Whittaker, A. C., & Boulton, S. J. (2012). Tectonic and climatic controls on knickpoint retreat
905 rates and landscape response times. *Journal of Geophysical Research: Earth Surface*,
906 117(F2), F02024. <https://doi.org/10.1029/2011JF002157>
- 907 Whittaker, A. C., Cowie, P. A., Attal, M., Tucker, G. E., & Roberts, G. P. (2007). Contrasting
908 transient and steady-state rivers crossing active normal faults: New field observations from
909 the Central Apennines, Italy. *Basin Research*, 19(4), 529–556.
910 <https://doi.org/10.1111/j.1365-2117.2007.00337.x>
- 911 Wobus, C. W., Whipple, K. X., Kirby, E., Snyder, N., Johnson, J., Spyropolou, K., et al. (2006a).
912 Tectonics from topography: Procedures, promise, and pitfalls. In Special Paper 398:
913 Tectonics, Climate, and Landscape Evolution (Vol. 398, pp. 55–74).
914 [https://doi.org/10.1130/2006.2398\(04\)](https://doi.org/10.1130/2006.2398(04))
- 915 Wobus, C. W., Crosby, B. T., & Whipple, K. X. (2006b). Hanging valleys in fluvial systems:
916 Controls on occurrence and implications for landscape evolution. *Journal of Geophysical*
917 *Research: Earth Surface*, 111(2), F02017. <https://doi.org/10.1029/2005JF000406>
- 918 Yanites, B. J. (2018). The dynamics of channel slope, width, and sediment in actively eroding
919 bedrock river systems. *Journal of Geophysical Research: Earth Surface*, 123(7), 1504–
920 1527. <https://doi.org/10.1029/2017JF004405>
- 921 Yanites, B. J., & Tucker, G. E. (2010). Controls and limits on bedrock channel geometry.
922 *Journal of Geophysical Research*, 115(F4), F04019. <https://doi.org/10.1029/2009JF001601>
- 923 Zhang, H., Kirby, E., Pitlick, J., Anderson, R. S., & Zhang, P. (2017). Characterizing the
924 transient geomorphic response to base-level fall in the northeastern Tibetan Plateau.
925 *Journal of Geophysical Research: Earth Surface*, 122(2), 546–572.
926 <https://doi.org/10.1002/2015JF003715>

Transient response and adjustment timescales of channel width and angle of valley-side slopes to accelerated incision

Naoya Takahashi^{1,*}, J. Bruce H. Shyu^{2,*}, Shinji Toda³, Yuki Matsushi⁴, Ryoga Ohta⁵, and Hiroyuki Matsuzaki⁶

¹ Department of Earth Science, Tohoku University, 6-3, Aramaki Aza-Aoba, Aoba-ku, Sendai 980-8578, Japan

² Department of Geosciences, National Taiwan University, No. 1, Sec. 4, Roosevelt Road, Taipei 106, Taiwan, ROC

³ International Research Institute of Disaster Science (IRIDeS), Tohoku University, Aoba, 468-1, Aoba, Sendai 980-0845, Japan

⁴ Disaster Prevention Research Institute, Kyoto University, Gokasho, Uji city, Kyoto 611-0011, Japan

⁵ Graduate School of Science, Kyoto University, Kitashirakawa Oiwake-cho, Kyoto city (JSPS Research Fellow), Kyoto 606-8502, Japan

⁶ Micro Analysis Laboratory, Tandem Accelerator (MALT), The University Museum, The University of Tokyo, 2-11-16, Yayoi, Bunkyo-ku, Tokyo 113-0032, Japan

Contents of this file

Tables S1, S3, and S4

Introduction

This document contains Tables S1, S3, and S4. Table S2 is provided separately.

Table S1
Basin Characteristics along the Yunodake Fault

Basin/ segment ID	Min. area (km ²)	Max. area (km ²)	θ^*	Ave k_{sn} (m ^{0.9})
1	0.025	24.1	0.19	28 ± 17
1-1	2.5	24.1	0.53	33 ± 16
1-2	0.025	2.5	0.34	11 ± 6
2	0.2	4.6	0.24	57 ± 19
2-1	0.2	4.6	0.46	62 ± 14
2-2	0.021	0.2	0.10	15 ± 5
3	1.0	6.9	0.11	69 ± 54
3-1	4.9	6.9	1.66	120 ± 46
3-2	0.021	4.7	0.48	31 ± 15
4	0.2	1.6	-1.05	61 ± 53
4-1	0.9	1.6	0.40	122 ± 21
4-2	0.1	0.9	-0.52	21 ± 11
5	0.3	3.4	0.26	83 ± 15
5-1	1.0	3.4	0.38	88 ± 11
5-2	0.4	1.0	0.88	57 ± 9
6	0.3	3.8	-0.69	64 ± 53
6-1	1.5	3.8	0.31	94 ± 44
6-2	0.3	1.4	0.68	12 ± 8

* Calculated by fitting channel slope and drainage area to equation (1).

Table S3*Results of ^{10}Be analysis in Abukuma Massif*

Sample ID	^{10}Be concentration ($\times 10^4$ atoms/g) ^d	Production rate (atoms/g yr) ^e	Erosion rate (g/m^2 yr)	Erosion rate (mm/yr) ^f	Upstream area (km^2)	Upstream ave. k_{sn} ($\text{m}^{0.9}$) ^g
ABK-R1 ^a	6.96 ± 0.36	7.3	219 ± 27	0.13 ± 0.02	7.6	45.9
ABK-R3 ^a	4.80 ± 0.22	6.8	296 ± 36	0.18 ± 0.02	97.2	30.1
Be1 ^b	5.22 ± 0.12	6.8	272 ± 31	0.17 ± 0.02	104.8	30.1
Be2 ^b	3.10 ± 0.09	6.1	412 ± 48	0.25 ± 0.03	24.1	47.6
Be3 ^b	5.05 ± 0.13	6.5	268 ± 31	0.16 ± 0.02	27.8	46.6
Be4 ^b	5.04 ± 0.12	7.1	296 ± 34	0.18 ± 0.02	161.3	35.0
Be5 ^b	4.49 ± 0.15	6.5	301 ± 35	0.18 ± 0.02	13.9	58.1
Be6 ^b	7.92 ± 0.16	6.7	178 ± 20	0.11 ± 0.01	101.6	17.5
Ab-21 ^c	5.86 ± 0.29	7.0	250 ± 31	0.15 ± 0.02	5.3	30.8

^a Nakamura et al. (2014). ^b Regalla et al. (2013). ^c Matsushi et al. (2014) ^d KNB5-1 ^{10}Be standard (Nishiizumi et al., 2007). ^e The production rate at sea level and high latitude was $4.68 \text{ atoms g}^{-1} \text{ yr}^{-1}$ corrected from the value proposed by Stone (2000) assuming a ^{10}Be half-life of 1.387 My (Chmeleff et al., 2010; Korshinek et al., 2010). ^f The bulk density of samples was $1.63 \text{ g}/\text{cm}^3$ (Nakamura et al., 2014). ^g Average k_{sn} for trunk and tributaries upstream from a sampling point.

Table S4*Erodibility Coefficient ($\text{m}^{0.1}/\text{yr}$) for Granitic Rocks in Iwaki and Abukuma Massif*

	$n = 2/3$	$n = 1$	$n = 5/3$	Reference
Iwaki	1.77E-05	4.85E-06	3.70E-07	This study
Abukuma	1.58E-05	4.52E-06	3.90E-07	Nakamura et al. (2014), Regalla et al. (2013), Matsushi et al. (2014)

Transient response and adjustment timescales of channel width and angle of valley-side slopes to accelerated incision

Naoya Takahashi^{1,*}, J. Bruce H. Shyu^{2,*}, Shinji Toda³, Yuki Matsushi⁴, Ryoga Ohta⁵, and Hiroyuki Matsuzaki⁶

¹ Department of Earth Science, Tohoku University, 6-3, Aramaki Aza-Aoba, Aoba-ku, Sendai 980-8578, Japan

² Department of Geosciences, National Taiwan University, No. 1, Sec. 4, Roosevelt Road, Taipei 106, Taiwan, ROC

³ International Research Institute of Disaster Science (IRIDeS), Tohoku University, Aoba, 468-1, Aoba, Sendai 980-0845, Japan

⁴ Disaster Prevention Research Institute, Kyoto University, Gokasho, Uji city, Kyoto 611-0011, Japan

⁵ Graduate School of Science, Kyoto University, Kitashirakawa Oiwake-cho, Kyoto city (JSPS Research Fellow), Kyoto 606-8502, Japan

⁶ Micro Analysis Laboratory, Tandem Accelerator (MALT), The University Museum, The University of Tokyo, 2-11-16, Yayoi, Bunkyo-ku, Tokyo 113-0032, Japan

Contents of this file

Figures S1 to S5

Introduction

This document contains Figures S1 to S5.

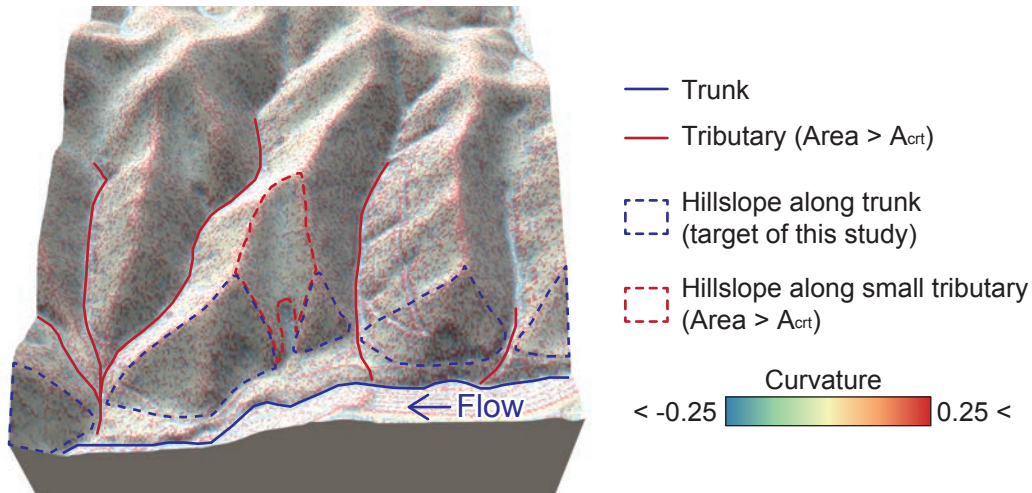


Figure S1. Results of hillslope mapping. Hillslopes along the trunk stream are used in the analysis. The base map is a shaded relief map colored by topographic curvature.

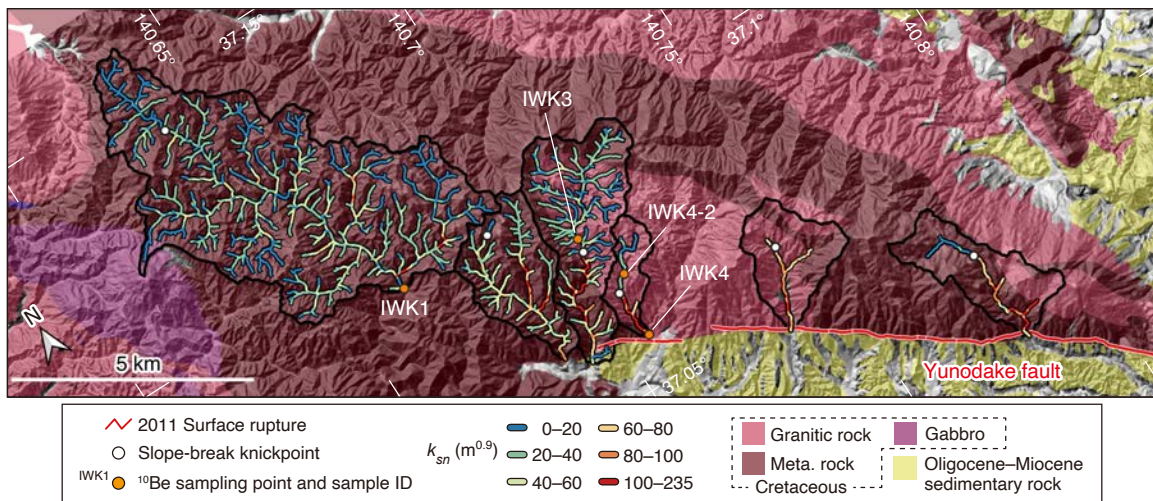


Figure S2. ^{10}Be sampling points and normalized channel steepness for the trunk and tributaries. The 2011 surface rupture trace is after Toda and Tsutsumi (2013). Geologic units are after Kubo et al. (2007) and Geological Survey of Japan (2020).

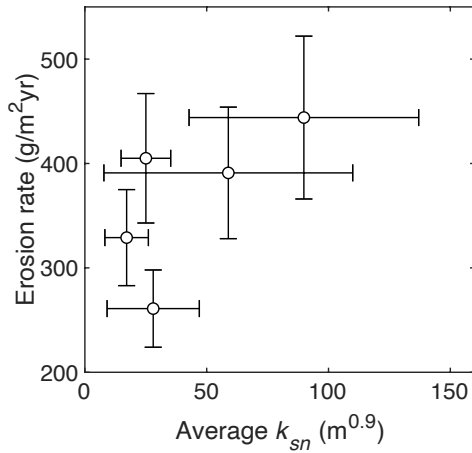


Figure S3. Basin-averaged erosion rates and average normalized channel steepness upstream of the ^{10}Be sampling points. Vertical and horizontal bars indicate 1 sigma error ranges.

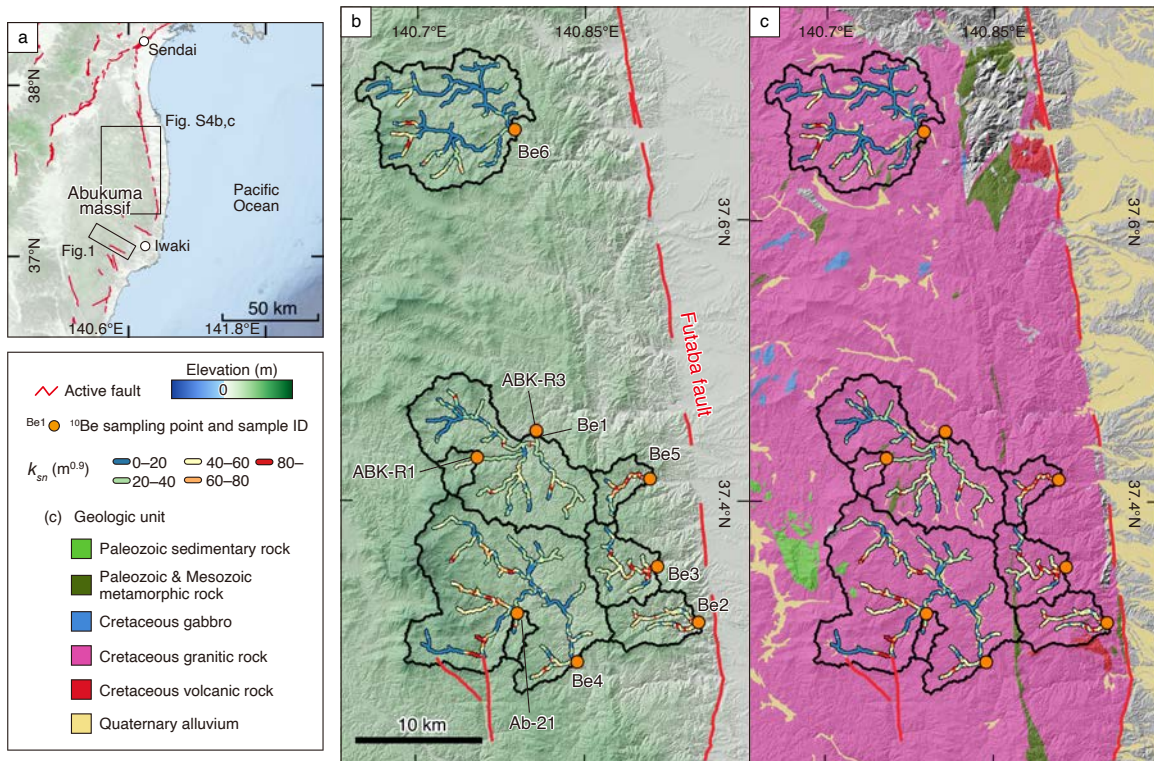


Figure S4. Normalized channel steepness and ^{10}Be samples in the Abukuma massif. (a) Topography and active faults around the Abukuma massif. (b) Normalized channel steepness and ^{10}Be samples. Results of the ^{10}Be analysis and references are shown in Table S2. (c) Geologic map (Geological Survey of Japan, 2020). Active fault traces are after Nakata and Imaizumi (2002).

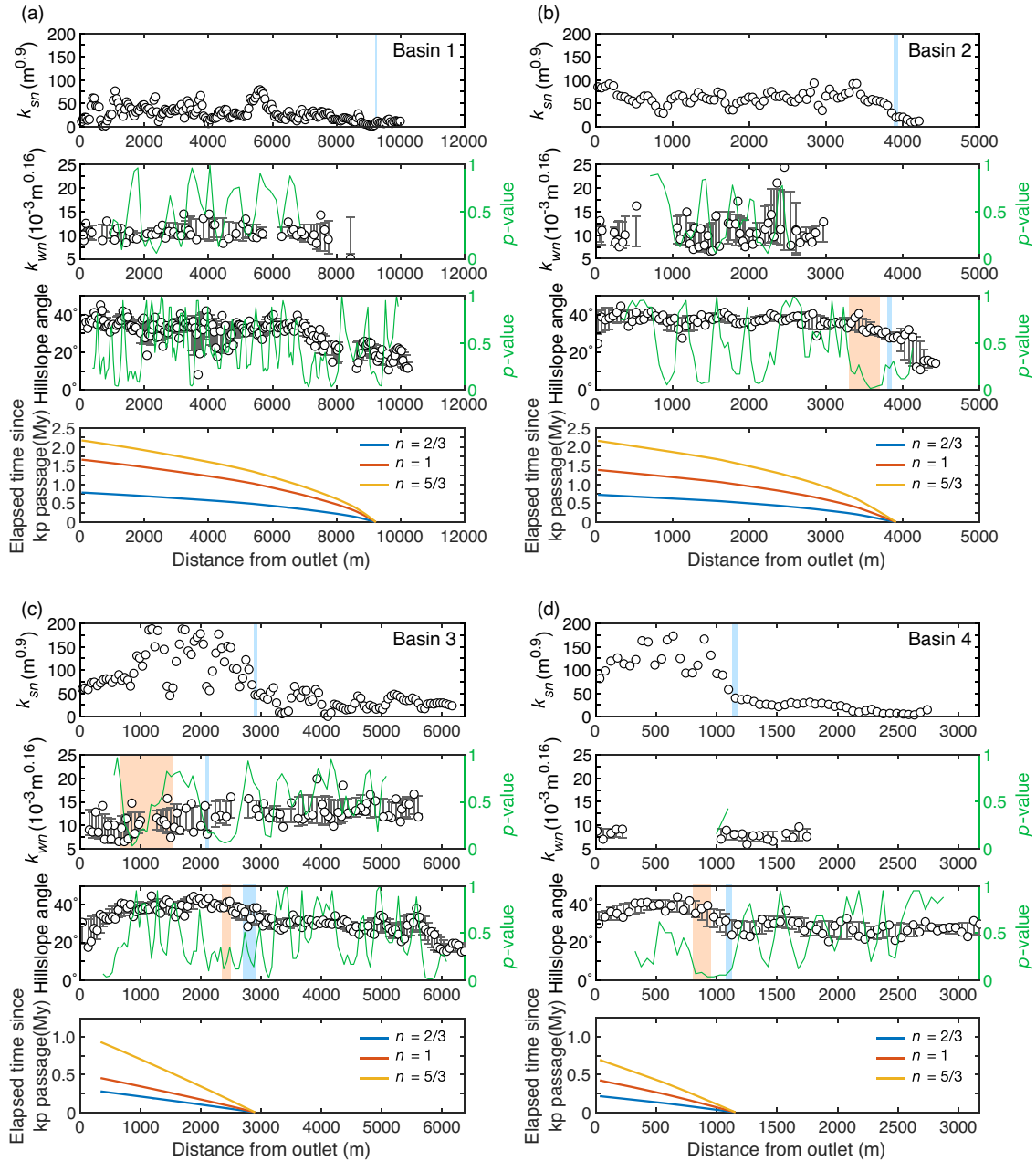


Figure S5. Along-trunk variations of channel and hillslope morphologies and knickpoint (kp) travel time in Basins 1–6. Average hillslope angle is calculated every 50 m along trunk streams. Gray bars in the upper and lower middle figures represent 8-point moving average and standard deviation. The green line in the upper middle figure indicates p -value of Student's t test. The green line in the lower middle figure indicates p -value of the Mann-Whitney U test. Blue and orange areas indicate sections where adjustment starts and finishes.

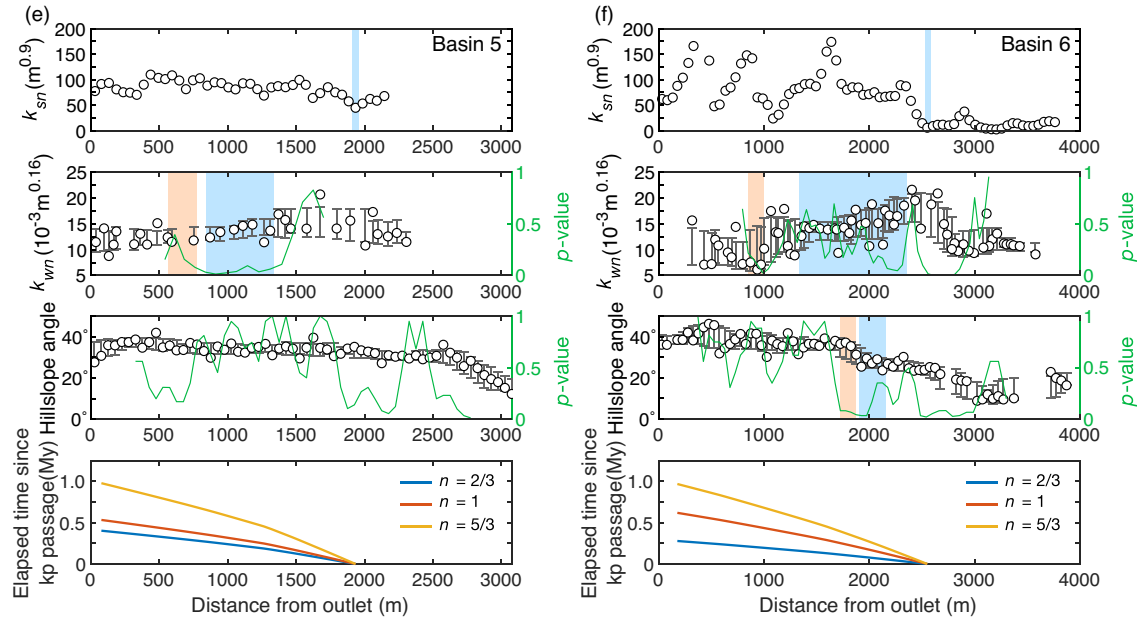


Figure S5. Continued.

Latitude (E)	Longitude (N)	Basin	Area (m ²)	Distance from outlet (m)	width (m)	width uncertainty (\pm , m)	flow depth (m)	flow depth uncertainty (\pm , m)
140.6414	37.1359	1	3308724	7740	5	1	0.5	0
140.6499	37.1200	1	9697008	4860	8.9	1.1	0.7	0
140.6471	37.1192	1	9624754	5160	11.5	1	0.85	0.05
140.6571	37.1087	1	14398559	2495	11.45	1.95	0.01	0.1
140.6422	37.1287	1	4546321	6755	6.25	0.15	0.7	0.1
140.6427	37.1258	1	4914795	6285	6.3	0.2	1.2	0.1
140.6438	37.1221	1	7619083	5685	8	0.3	0.6	0.1
140.6444	37.1218	1	7632594	5620	8.15	0.15	0.5	0.1
140.6456	37.1202	1	7853117	5390	7.55	0.15	0.8	0.1
140.6646	37.0935	1	23956273	295	13.6	0.2	0.9	0.1
140.6428	37.1337	1	3981009	7375	4.9	0.1	0.7	0.1
140.6429	37.1298	1	4383003	6900	6.6	0.1	0.8	0.1
140.6462	37.1194	1	7893658	5245	8.8	0.1	0.6	0.1
140.6571	37.1049	1	14998044	2025	9.95	0.45	0.7	0.1
140.6571	37.1075	1	14578487	2350	10.4	0.6	1	0.1
140.6624	37.0969	1	19837173	820	15.1	0.5	1.1	0.1
140.6515	37.1191	1	11240483	4630	8.5	0.5	0.6	0.1
140.6567	37.1118	1	13843767	2910	10.7	0.3	0.8	0.1
140.6558	37.1137	1	13684863	3150	9.85	0.15	0.7	0.1
140.6418	37.1280	1	4571816	6655	7	0.1	0.95	0.15
140.6416	37.1354	1	3320389	7625	6.1	0.1	0.75	0.15
140.6624	37.0986	1	19280323	1030	12.15	0.65	0.95	0.15
140.6617	37.1018	1	19103742	1415	9.6	0.1	0.95	0.15
140.6542	37.1177	1	11967646	4195	11.5	0.1	0.95	0.15
140.6572	37.1106	1	13905837	2760	10.8	0.6	1.15	0.15
140.6576	37.1099	1	14228164	2655	9.5	0.1	0.85	0.15
140.6621	37.1007	1	19141110	1280	13.1	0.8	0.7	0.2
140.6553	37.1146	1	13588868	3280	11.3	0.2	1.1	0.2
140.6643	37.0919	1	24004851	105	11.15	0.75	1.1	0.2
140.6480	37.1193	1	9646482	5075	10.65	0.85	0.9	0.2
140.6450	37.1211	1	7688725	5510	7.4	0.3	0.7	0.2
140.6645	37.0909	1	24098780	0	14.95	0.25	1	0.2
140.6420	37.1346	1	3338568	7505	7.85	0.55	1.1	0.2
140.6592	37.1038	1	17300336	1755	10.1	0.1	0.8	0.2
140.6599	37.1032	1	17347565	1655	10.25	0.55	1	0.2
140.6627	37.0958	1	19896455	690	10.35	0.55	0.7	0.2
140.6610	37.1025	1	17398887	1520	11.9	0.3	0.8	0.2
140.6624	37.0996	1	19177671	1155	13.1	0.1	1.1	0.2
140.6554	37.1176	1	11993823	4020	13.6	0.3	1.1	0.2
140.6561	37.1128	1	13723230	3050	9.9	0.1	1.4	0.2
140.6539	37.1156	1	13299245	3625	8.9	0.4	0.8	0.2
140.6428	37.1306	1	4349641	6990	6.2	0.8	0.75	0.25
140.6375	37.1402	1	2610286	8435	2.5	1	0.75	0.25
140.6418	37.1275	1	4577308	6590	6.8	0.1	1.55	0.25
140.6428	37.1332	1	4198735	7295	6.1	0.3	0.85	0.25
140.6425	37.1326	1	4213944	7220	5.4	0.5	1.15	0.25
140.6569	37.1064	1	14603660	2220	10.3	0.1	0.95	0.25
140.6538	37.1148	1	13303144	3445	9.9	0.1	0.95	0.25
140.6644	37.0924	1	24008208	165	15.75	0.25	1	0.3
140.6643	37.0917	1	24040634	85	12.65	0.35	0.9	0.3
140.6573	37.1091	1	14376733	2555	12.3	0.2	0.9	0.3
140.6571	37.1081	1	14403072	2425	11.4	0.4	1	0.3
140.6646	37.0940	1	20017949	350	12.3	0.7	1.2	0.3

140.6623	37.0989	1	19249199	1065	10.3	0.3	0.8	0.3
140.6523	37.1177	1	11910837	4455	7.75	0.25	1	0.3
140.6554	37.1168	1	13257232	3835	13.3	0.7	1	0.4
140.6414	37.1267	1	4734345	6490	8.15	1.35	1.1	0.44
140.6544	37.1180	1	11983181	4155	11.45	1.75	1.2	0.5
140.6543	37.1146	1	13552123	3380	10.85	0.55	1.3	0.5
140.6569	37.1053	1	14844375	2080	10.6	1	1.2	0.6
140.6556	37.1142	1	13688090	3225	14.4	0.4	1.35	1.15
140.6827	37.0808	2	1294430	2605	4.1	0.3	1	0.1
140.6878	37.0736	2	3826125.9	1460	5.75	0.15	1.7	0.1
140.6880	37.0729	2	3870734	1365	6.65	0.55	1.5	0.1
140.6881	37.0722	2	3895254	1270	4.1	0.3	0.7	0.1
140.6881	37.0719	2	3907132	1230	6	0.1	0.7	0.1
140.6867	37.0755	2	1856689	1725	5.4	1	0.8	0.1
140.6874	37.0741	2	3364863	1520	3.7	0.2	0.5	0.1
140.6876	37.0739	2	3794934	1495	3.8	0.2	0.8	0.1
140.6881	37.0718	2	3907132	1225	4.8	0.6	0.7	0.1
140.6877	37.0663	2	4504252	350	5.3	0.9	0.8	0.1
140.6876	37.0663	2	4514968	305	4.7	0.3	0.9	0.1
140.6845	37.0794	2	1594915	2320	3.9	0.1	0.8	0.1
140.6852	37.0792	2	1703111	2245	5.2	0.4	0.8	0.1
140.6854	37.0789	2	1727083	2205	4.7	0.3	0.6	0.1
140.6855	37.0784	2	1747590	2130	3.6	0.2	0.8	0.1
140.6825	37.0812	2	1195143	2660	3	0.3	0.6	0.1
140.6826	37.0809	2	1197940	2610	3.9	0.3	0.9	0.1
140.6828	37.0804	2	1526529	2540	3.1	0.1	0.6	0.1
140.6855	37.0780	2	1766827	2095	4.35	0.45	0.7	0.1
140.6857	37.0778	2	1772874	2045	3.4	0.2	0.6	0.1
140.6859	37.0775	2	1785656	2005	4.4	0.5	0.7	0.1
140.6819	37.0828	2	1121721	2860	3.65	0.35	0.6	0.1
140.6820	37.0825	2	1160326	2815	3	0.4	0.6	0.1
140.6821	37.0822	2	1168761	2785	3.4	0.1	0.8	0.1
140.6841	37.0796	2	1597571.8	2360	8.5	0.1	1.85	0.15
140.6880	37.0663	2	4500153.1	380	6.25	1.15	2.25	0.15
140.6873	37.0743	2	3406932.8	1565	7.8	0.1	2.95	0.15
140.6872	37.0660	2	4527040	255	5.3	0.5	0.75	0.15
140.6838	37.0798	2	1569351	2405	4.5	0.2	0.75	0.15
140.6861	37.0771	2	1797879	1945	3.2	0.3	0.75	0.15
140.6822	37.0837	2	972554	2965	4.2	0.1	0.55	0.15
140.6880	37.0724	2	3870734	1290	6.75	0.35	2	0.2
140.6892	37.0668	2	4394018	530	10	0.5	1	0.2
140.6872	37.0748	2	3328024	1610	4.2	0.3	0.6	0.2
140.6871	37.0659	2	4545847	240	6.6	0.5	0.7	0.2
140.6871	37.0643	2	4583548	55	8.2	0.4	1.2	0.2
140.6861	37.0769	2	1810704	1915	3.7	0.5	0.8	0.2
140.6865	37.0757	2	1851546	1745	5.3	0.7	0.7	0.2
140.6823	37.0819	2	1179305	2740	3.4	0.7	0.8	0.2
140.6849	37.0793	2	1703272.7	2285	5.95	0.15	1.45	0.25
140.6878	37.0727	2	3873735	1340	4.4	0.4	0.65	0.25
140.6882	37.0708	2	4145042	1100	5.5	0.5	0.95	0.25
140.6879	37.0733	2	3842232	1415	4.6	1.6	0.6	0.3
140.6871	37.0645	2	4577092	80	6.9	0.1	1.5	0.3
140.6863	37.0764	2	1811177.8	1850	7.3	0.1	1.45	0.35
140.6864	37.0760	2	1843649	1820	5.3	1.3	0.85	0.35
140.6863	37.0766	2	1820473	1875	4.4	0.6	1.1	0.4
140.6882	37.0716	2	3904754.9	1185	8.75	0.05	3.25	0.45

140.6873	37.0662	2	4536126.9	290	5.6	0.4	1.55	0.55
140.6882	37.0705	2	4200503	1060	7	0.2	1.45	0.75
140.6834	37.0799	2	1537922.2	2455	9.7	2.2	1.8	1
140.6962	37.0707	3	5898270	1420	7.1	0.1	0.85	0.05
140.7125	37.0892	3	2352413	5025	5.6	0.1	0.55	0.05
140.7131	37.0897	3	1850815	5110	5.15	0.05	0.55	0.05
140.7104	37.0876	3	2473778	4730	6.3	0.5	0.55	0.05
140.7110	37.0881	3	2426911	4810	7.95	0.25	0.65	0.05
140.7116	37.0885	3	2383658	4895	7.25	0.05	0.85	0.05
140.7135	37.0913	3	1022951	5310	3.6	0.2	0.55	0.05
140.7095	37.0851	3	2941119	4275	6.65	0.05	0.65	0.05
140.7083	37.0842	3	3371319	4110	6.6	0.1	0.75	0.05
140.7043	37.0818	3	4307440.2	3500	9.05	0.55	0.85	0.05
140.6930	37.0619	3	6716988	195	6.35	0.15	0.9	0.1
140.6966	37.0702	3	5927040	1330	7.6	0.1	0.7	0.1
140.7131	37.0901	3	1788066	5160	4.9	0.1	0.5	0.1
140.7165	37.0918	3	744715	5605	3.45	0.15	0.4	0.1
140.7052	37.0805	3	4417392	3310	7.65	0.25	0.6	0.1
140.7035	37.0781	3	4841621	2960	7.7	0.2	0.6	0.1
140.7046	37.0796	3	4634590	3205	8	0.5	0.6	0.1
140.7158	37.0917	3	793692	5535	5	0.2	0.5	0.1
140.7150	37.0916	3	837159	5455	4.45	0.05	0.4	0.1
140.7137	37.0914	3	1022951	5330	4.5	0.1	0.8	0.1
140.7133	37.0906	3	1753550	5235	6.55	0.25	0.5	0.1
140.7097	37.0855	3	2936062	4330	6.2	0.1	0.7	0.1
140.7094	37.0865	3	2906345	4440	6.55	0.25	0.4	0.1
140.7094	37.0868	3	2900072	4565	6.8	0.2	0.5	0.1
140.7058	37.0838	3	3942294	3850	7.2	0.3	0.7	0.1
140.7087	37.0844	3	3365939	4155	6.3	0.3	0.9	0.1
140.7066	37.0839	3	3535936	3925	11.2	1	0.4	0.1
140.7050	37.0800	3	4536687.1	3260	7.9	0.1	0.6	0.1
140.7041	37.0825	3	4224177	3610	6.95	0.15	0.5	0.1
140.7048	37.0830	3	4124839.5	3690	6.8	0.2	1.1	0.1
140.7045	37.0793	3	4644569.1	3135	7.3	0.2	0.8	0.1
140.6932	37.0623	3	6704268.3	250	9.45	0.25	0.01	0.1
140.6960	37.0709	3	5899700	1440	10.95	0.15	1.1	0.1
140.6941	37.0630	3	6640856	365	10.4	1	0.01	0.1
140.6952	37.0659	3	6255185.3	755	8.15	0.15	1.9	0.1
140.6944	37.0632	3	6620069	400	5.15	0.45	0.75	0.15
140.6953	37.0649	3	6394511	635	4.75	0.25	0.75	0.15
140.6950	37.0639	3	6587952	505	5.2	0.2	0.85	0.15
140.7144	37.0916	3	846670	5400	4.5	0.5	0.65	0.15
140.6958	37.0712	3	5878451	1495	5.2	0.2	1	0.2
140.6997	37.0736	3	5429703	2100	5.5	0.1	1.1	0.2
140.6958	37.0675	3	6104440	965	7.25	0.45	0.6	0.2
140.7051	37.0809	3	4334233	3360	5.95	0.05	0.7	0.2
140.7079	37.0839	3	3392881	4050	7.1	0.1	0.8	0.2
140.7098	37.0874	3	2804691	4675	6.7	0.2	0.5	0.2
140.7105	37.0877	3	2486284	4745	7.1	1	0.6	0.2
140.7074	37.0838	3	3409800.9	4010	8	0.1	1.1	0.2
140.7091	37.0846	3	3174725.5	4200	5.3	0.5	1	0.2
140.7015	37.0739	3	5196032.5	2320	8	0.2	1.8	0.2
140.7016	37.0753	3	5126678	2495	10.55	0.85	0.9	0.2
140.6959	37.0720	3	5787847.8	1600	8.75	0.65	1.2	0.2
140.6967	37.0729	3	5669979.7	1750	9.35	0.35	2.3	0.2
140.7034	37.0768	3	4940907.9	2790	10.15	0.15	0.8	0.2

140.7033	37.0778	3	4849706.7	2915	8.65	0.65	1.1	0.2
140.7039	37.0787	3	4723068.9	3040	9.3	0.2	1.1	0.2
140.7052	37.0835	3	3946647	3780	7.2	0.1	0.9	0.2
140.6926	37.0615	3	6767403.8	145	6.7	1	1.7	0.2
140.6967	37.0696	3	5935793.6	1265	8.1	0.8	1.1	0.2
140.6953	37.0662	3	6244268	790	5.1	1.1	0.75	0.25
140.7095	37.0872	3	2892702	4650	7.1	0.5	0.65	0.25
140.6958	37.0716	3	5804772	1555	6.65	0.95	0.9	0.3
140.6966	37.0705	3	5905866	1380	7.7	1	0.9	0.3
140.6990	37.0730	3	5458882	1995	6.7	0.3	1	0.3
140.6978	37.0731	3	5495334	1875	5.8	0.5	0.8	0.3
140.6953	37.0657	3	6280473	725	4.7	0.4	1	0.3
140.6946	37.0635	3	6613613	450	7.3	0.5	0.9	0.3
140.6954	37.0671	3	6194839	900	5.9	0.2	0.8	0.3
140.7098	37.0857	3	2946423.9	4355	9.65	0.25	0.9	0.3
140.7017	37.0747	3	5196032.5	2420	7.85	0.75	2.1	0.3
140.6975	37.0732	3	5556673.5	1840	9.95	0.55	1.6	0.3
140.6951	37.0643	3	6499995.2	555	7.3	0.2	1.8	0.3
140.6953	37.0653	3	6373465.9	680	6.8	0.2	1.9	0.3
140.6961	37.0724	3	5782909	1650	6.2	0.2	1.05	0.35
140.6960	37.0677	3	6102349.9	995	7.8	0.2	1.95	0.35
140.7009	37.0735	3	5343339.6	2235	7.85	0.65	1.3	0.4
140.6951	37.0668	3	6206045	850	10.5	0.3	1.5	0.4
140.6935	37.0625	3	6688885	295	6.3	0.1	1.4	0.7
140.6994	37.0734	3	5434437.1	2065	9.55	0.75	2.25	0.75
140.7060	37.0606	4	1535653	125	3.3	0.3	0.55	0.05
140.7059	37.0690	4	906589	1210	2.6	0.1	0.45	0.05
140.7063	37.0691	4	853621	1250	1.85	0.05	0.45	0.05
140.7078	37.0708	4	797457	1575	2.5	0.1	0.55	0.05
140.7082	37.0711	4	767471	1630	2.2	0.1	0.35	0.05
140.7073	37.0701	4	826249	1420	2.15	0.05	0.45	0.05
140.7075	37.0705	4	801869	1465	2	0.2	0.55	0.05
140.7063	37.0596	4	1553438	10	3.5	0.5	0.7	0.1
140.7055	37.0612	4	1446986	220	3.55	0.35	0.7	0.1
140.7058	37.0608	4	1509411	170	3.6	0.2	0.6	0.1
140.7061	37.0680	4	951681	1080	2.9	0.1	0.4	0.1
140.7059	37.0685	4	941255	1145	2.6	0.2	0.4	0.1
140.7061	37.0677	4	959299	1035	2.3	0.2	0.4	0.1
140.7093	37.0714	4	721411	1745	2.2	0.2	0.5	0.1
140.7068	37.0693	4	844938	1300	2.4	0.2	0.5	0.1
140.7071	37.0696	4	837159	1350	2.4	0.2	0.4	0.1
140.7086	37.0712	4	729674	1680	2.8	0.1	0.65	0.15
140.7062	37.0600	4	1544949	60	2.8	0.2	0.8	0.2
140.7390	37.0535	5	2370076	1110	6.95	0.05	0.85	0.05
140.7402	37.0548	5	2234767	1310	6.35	0.45	1.05	0.05
140.7369	37.0495	5	3102455	560	6.6	0.2	0.95	0.05
140.7414	37.0626	5	367425	2305	2.5	0.1	0.5	0.1
140.7413	37.0620	5	405436	2235	3	0.1	0.6	0.1
140.7414	37.0614	5	423421	2170	2.9	0.1	0.4	0.1
140.7414	37.0586	5	1016366	1795	4.7	0.7	0.9	0.1
140.7411	37.0568	5	1073498	1575	4.8	0.7	0.7	0.1
140.7420	37.0607	5	639941	2060	4.75	0.15	0.7	0.1
140.7393	37.0541	5	2359030	1180	7.05	0.05	1	0.1
140.7406	37.0557	5	1208936	1420	5.65	0.15	1.1	0.1
140.7405	37.0552	5	1212906	1370	6.05	0.05	1.1	0.1
140.7363	37.0481	5	3191251	360	7.05	0.45	1.4	0.1

140.7376	37.0507	5	2837382	750	6.05	0.45	1.2	0.1
140.7356	37.0467	5	3305687	165	6	0.2	1	0.1
140.7418	37.0609	5	631100	2095	3.55	0.15	0.45	0.15
140.7421	37.0603	5	949196	2005	3.5	0.1	0.45	0.15
140.7354	37.0465	5	3312875	130	4.8	0.5	0.85	0.15
140.7357	37.0468	5	3301577	185	7.4	0.8	1.1	0.2
140.7412	37.0576	5	1033280	1675	6.95	0.15	0.75	0.25
140.7416	37.0595	5	965787	1895	5.1	0.5	0.85	0.25
140.7347	37.0459	5	3341322	35	6.3	0.1	1.15	0.25
140.7352	37.0463	5	3327916	95	7.75	0.25	0.85	0.25
140.7364	37.0477	5	3247641	315	6	0.6	0.95	0.25
140.7382	37.0517	5	2792834	870	6.3	0.3	1.05	0.25
140.7386	37.0531	5	2407608	1045	6.65	0.15	1.2	0.3
140.7362	37.0485	5	3157941	410	5.9	0.3	1.3	0.3
140.7370	37.0498	5	3062484	590	6.1	0.5	1.3	0.3
140.7408	37.0560	5	1204449	1460	5.05	0.15	0.9	0.4
140.7383	37.0523	5	2571722	945	6.6	0.8	1.2	0.4
140.7397	37.0547	5	2330283	1265	5.4	0.4	1.1	0.4
140.7365	37.0490	5	3137767	485	8.1	0.4	1.1	0.4
140.7817	37.0231	6	3666963	430	4.05	0.25	0.95	0.05
140.7809	37.0259	6	3006880	795	3.8	0.1	0.95	0.05
140.7803	37.0368	6	1549769	2490	5.6	0.4	0.65	0.05
140.7803	37.0364	6	1562121	2435	7.8	0.4	0.95	0.05
140.7779	37.0410	6	1266843	3085	3.8	0.2	0.55	0.05
140.7770	37.0429	6	1089529	3345	3.8	0.1	0.55	0.05
140.7815	37.0236	6	3643185	500	4.1	0.2	0.8	0.1
140.7796	37.0268	6	2940086	1000	5.3	0.1	1.1	0.1
140.7791	37.0274	6	2851903	1190	9.2	0.5	1.1	0.1
140.7806	37.0265	6	2997584	870	3.95	0.45	0.7	0.1
140.7795	37.0316	6	1914983	1810	5.75	0.55	1.2	0.1
140.7793	37.0310	6	2444179	1690	6.7	0.5	1.3	0.1
140.7802	37.0361	6	1570556	2405	8.65	0.25	0.7	0.1
140.7796	37.0345	6	1711503	2190	6.9	1.1	0.7	0.1
140.7776	37.0418	6	1203062	3170	4.3	0.2	0.5	0.1
140.7767	37.0432	6	1076790	3370	3.7	0.2	0.5	0.1
140.7771	37.0427	6	1104549	3305	3.8	0.2	0.5	0.1
140.7755	37.0443	6	643944	3580	2.5	0.2	0.3	0.1
140.7765	37.0434	6	975244	3430	3.5	0.1	0.4	0.1
140.7773	37.0421	6	1148103	3215	4.6	0.2	0.6	0.1
140.7810	37.0227	6	3713250	315	9	0.2	0.65	0.15
140.7790	37.0268	6	2876133	1110	6.9	0.7	0.45	0.15
140.7800	37.0268	6	2943744	970	3.7	0.5	0.85	0.15
140.7815	37.0242	6	3633330	565	6.15	0.55	0.55	0.15
140.7803	37.0268	6	2950329	935	3.2	0.2	0.65	0.15
140.7814	37.0251	6	3041052	690	4.5	0.5	0.95	0.15
140.7795	37.0311	6	2426222	1705	4.5	0.1	0.75	0.15
140.7803	37.0377	6	1516243	2590	7.4	0.1	0.65	0.15
140.7797	37.0337	6	1860283	2085	6.5	0.5	0.75	0.15
140.7796	37.0342	6	1775091	2150	7.4	0.1	1.15	0.15
140.7787	37.0403	6	1365484	2945	3.7	0.3	0.55	0.15
140.7783	37.0405	6	1342717	2995	3.5	0.1	0.45	0.15
140.7773	37.0425	6	1129640	3280	3.9	0.5	0.55	0.15
140.7790	37.0399	6	1395825	2895	4.2	0.5	0.55	0.15
140.7802	37.0381	6	1497952	2650	8.2	0.2	0.65	0.15
140.7798	37.0385	6	1457024	2710	5.8	0.7	0.55	0.15
140.7796	37.0387	6	1450052	2740	5	0.3	0.85	0.15

140.7792	37.0266	6	2935395	1065	9.1	0.1	0.8	0.2
140.7788	37.0279	6	2834731	1250	4.7	0.3	1.1	0.2
140.7790	37.0271	6	2855002	1135	6.8	0.5	0.9	0.2
140.7811	37.0254	6	3029023	730	7.6	0.1	0.8	0.2
140.7815	37.0239	6	3638408	535	6.8	0.1	0.6	0.2
140.7796	37.0313	6	1917307	1760	6.2	0.4	0.9	0.2
140.7796	37.0322	6	1906160	1870	7.7	0.7	0.9	0.2
140.7785	37.0289	6	2793157	1380	7.4	0.1	1.1	0.2
140.7785	37.0286	6	2811448	1355	6.45	0.05	1.1	0.2
140.7785	37.0305	6	2454347	1605	6.7	0.1	0.9	0.2
140.7795	37.0333	6	1870138	2025	8.1	0.1	0.9	0.2
140.7793	37.0331	6	1874055	2000	4.6	0.4	1.2	0.2
140.7793	37.0393	6	1413062	2810	4.3	0.9	0.7	0.2
140.7792	37.0396	6	1407747	2845	3.7	0.1	0.7	0.2
140.7796	37.0325	6	1895315	1920	6.4	0.5	1.25	0.25
140.7787	37.0291	6	2720381	1430	7.15	0.05	0.85	0.25
140.7786	37.0282	6	2823369	1290	4.55	0.35	0.85	0.25
140.7784	37.0299	6	2681304	1530	7.05	0.55	1.35	0.25
140.7798	37.0356	6	1610882	2330	7.5	0.6	0.95	0.25
140.7796	37.0352	6	1684002	2265	6.8	0.2	0.85	0.25
140.7778	37.0416	6	1257676	3140	3.9	0.5	0.65	0.25
140.7778	37.0414	6	1259828	3115	6.2	1	0.55	0.25
140.7794	37.0391	6	1438389	2785	3.9	0.1	0.65	0.25
140.7815	37.0248	6	3050132	655	5	0.1	1.1	0.3
140.7794	37.0328	6	1884211	1965	6.55	0.75	1.5	0.3
140.7795	37.0318	6	1912100	1830	6.8	0.8	1	0.3
140.7791	37.0309	6	2444179	1670	6.8	0.7	1.1	0.3
140.7797	37.0340	6	1850212	2130	4.7	0.2	1	0.3
140.7796	37.0349	6	1701002	2235	6.15	0.15	1	0.3
140.7790	37.0276	6	2847104	1225	5.5	1	0.95	0.35
140.7787	37.0294	6	2711559	1470	7.45	1.25	1.3	0.6